Chapter 3

Electrochemistry, Spectroelectrochemistry and Monolayer Formation of Mononuclear Ruthenium and Osmium Polypyridyl Complexes

Four mononuclear complexes of the type $[M(bipy)_2L]^{2+}$ where M is Ru/Os, bipy is 2,2'-bipyridyl and L represents either the ligand 2-(4-pyridyl)imidazole[f]-1,10-phenanthroline (pyrphen) or 2-(3-thio)imidazole[f]-1,10-phenanthroline (thimphen) have been studied as potential components for molecular electronic devices. Cyclic voltammetry and differential pulse voltammetry reveal a reversible one-electron metal centred oxidation and several ligand based reductions for each complex, the peak potentials of which are solvent dependent. Cyclic voltammetry and reductive spectroelectrochemistry of the M(pyrphen) complex suggest that the LUMO is based on the pyrphen unit itself whereas the same experiments imply that the LUMO of the M(thimphen) complexes is centred on a bipyridyl ligand. In contrast to this excited state Raman spectroscopy provides evidence for a lowest lying excited state where the π^* orbital is bipy based for both types of complexes. Monolayers of each of the four complexes have been formed on Au and Pt substrates. Initial analysis suggests that repulsive interactions exist between adsorbates on the surface and the projected area per molecule, calculated from the surface coverage, indicates that these complexes do not form complete monolayers on the surface. This is most likely due to the existence of lateral interactions within the monolayer.

3.1 Introduction

Ruthenium and osmium are transition metals belonging to group VIII of the d-block of the periodic table. Situated directly below iron, in rows two and three respectively, these noble metals exhibit properties which are quite different to those of iron. These heavier metals are relatively inert in that they do not react with mineral acids including aqua regia (a mixture used to dissolve metals that consist of concentrated hydrochloric acid mixed with concentrated nitric acid) at temperatures below 100ºC. Also, in contrast to iron, ruthenium and osmium may be considered as precious metals due to their rarity in the earth's crust.[1, 2]

Ruthenium, depending on the coordinating ligands within the complex, can exist in nine different oxidation states (0-8) with osmium known to exist in eight (0, 2-8).[3] The complexes discussed in this chapter are M-N_6 complexes (M = Ru/Os) where the ground state has an oxidation number of 2+. Complexes of ruthenium and osmium exhibit particularly interesting electrochemical and photophysical properties, especially those of the d^6 complexes of each metal. Over the last half a century more and more scientists have expressed interest in the rich and diverse chemistry of these coordination complexes. Owing to the extensive research that has been carried out on the chemistry of ruthenium and osmium polypyridyl compounds, ample understanding now surrounds their robust ligand chemistry and the synthetic strategies associated with them. There are several exciting and interesting attractions in the chemistry of these octahedral group VIII metal complexes, in particular the ability to tune the electrochemical and photophysical properties through variation of the coordinated ligands.[4] The first reporting of the luminescence properties of the parent ion, $[Ru(bipy)_3]^{2+}$ (where bipy = 2,2'-bipyridine), in 1959 by Paris and Brandt [5] sparked incredible curiosity regarding these systems and, through the years to this day this interest has flourished.

3.1.1 Mononuclear Transition Metal Complexes in Molecular Electronics

As discussed in Chapter 1, the area of semiconductors has experienced a remarkable miniaturization trend, in particular in the last 50 years or so.[6] Moore's law states that

in order to progress in the semiconductor industry the number of transistors per chip would need to double, by reducing the functional area by a half every couple of years, with each new technology generation.[7]

Finite limits exist in the downscaling of solid state silicon based integrated circuits.[8] Such limits are fast approaching and it is this which drives the search for novel ways of achieving the desired miniaturization targets in the semi-conductor industry. Molecular electronics is concerned with using one or more molecules mounted on a surface as a means of replacing electronic devices, such as transistors, wires and diodes [8], a concept that was born from Richard P. Feynman [9] in an address entitled "*There is plenty of room at the bottom*". The concept of the "bottom-up" approach has led to a considerable amount of research surrounding organic and inorganic systems in the area of molecular wires [6c, 7, 8, 10], transistors [11] and diodes.[12] This chapter focuses on mononuclear transition metal complexes and their potential use as 'transistor-like' components for molecular electronic devices.

Molecules are said to have transistor-like behaviour when the properties of the molecule can be alternated between conducting and insulating through a change in the physical, electronic or magnetic structure once an external gate signal has been applied. Alternating between these two states allows control of the flow of electrons, acting like a switch in that the conducting state allows current to flow where the insulating state does not. In order to design such a system one must have the ability to control the organization and function of the molecule when assembled in a monolayer on a surface. Interfacial electron transfer and molecular conductivity between the molecule and the electrode surfaces are key issues when creating a molecular electronic device. There are major limitations, unfortunately, with those molecular "transistors" that have been reported previously in the literature in that cryogenic temperatures or ultra-high vacuums are required for their operation.[11b, c] However, systems comprised of mononuclear osmium and cobalt complexes, Figure 3.1, assembled on platinum and gold surfaces, have been reported as exhibiting transistor-like behaviour at room temperature in aqueous solutions.[13]

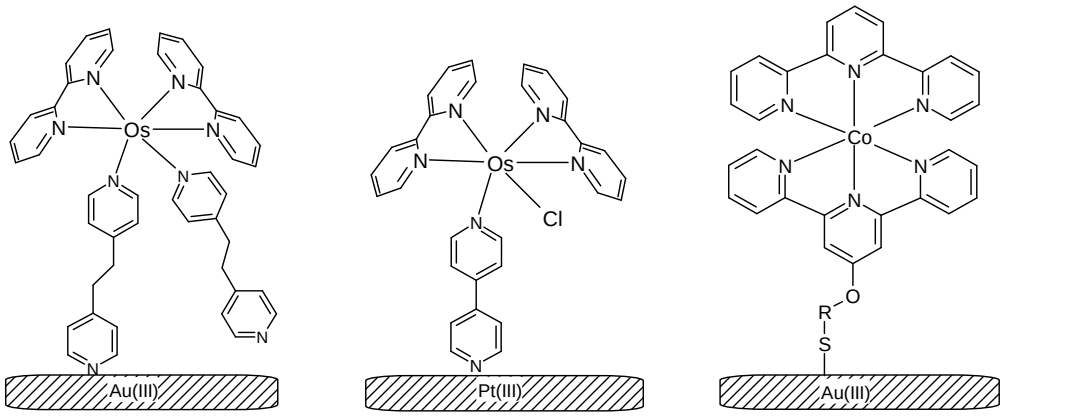

$[Os(bipy)_2(p2p)_2]^{2+/3+}$ **$[Os(bipy)_2(p0p)Cl]^{+/2+}$** **$[Co(tpy)(tpy\text{-}O\text{-}(CH_2)_6\text{-}SAc]^{+/2+}$**

Figure 3.1: *Molecular structures of the Os and Co complexes bound to Pt and Au surfaces where bipy = 2,2'-bipyridine, p0p = 4,4'-bipyridine, tpy = 2,2',2"-terpyridine and Ac = acetyl).*[13, 14]

These complexes prove beneficial in the quest for designing molecular electronic devices because 1) they have two robust redox states that are reversible and easily accessible, 2) their equilibrium redox potentials are within a desired range for assembly on Pt and Au surfaces as well as their insertion into a nanoscale environment such as scanning tunnelling microscopy (STM) and 3) there is extensive literature available regarding their synthesis and the electrochemical properties can be tuned by varying the coordinated ligands – the chemistry of which is robust and very well understood.[13c]

A key prerequisite in determining if these systems behave in a manner such that they can be deemed potentially useful for molecular electronic devices is the understanding of how these molecules function on a surface. In the mid 1990's, Forster et al. [14, 15] carried out extensive research into the synthesis, assembly and characterisation of these and other osmium complexes and their monolayers. These complexes form stable monolayers on metal surfaces and within this controlled environment electron transfer rates for these types of osmium complexes as high as 9.0 x 10^5 sec^{-1} (k^0_{ET}) have been reported.[16] The near ideal cyclic voltammetry of the $[Os(bipy)_2(p2p)Cl]^{2+}$ monolayer, where p2p is 1,2-bis(4-pyridyl)-ethane ($E_{pa} - E_{pc}$ = 35 mV and a full width at half maximum (FWHM) of 90-110 mV is observed) and the fast electron transfer kinetics suggest that the associated mechanisms for these types of osmium complexes

on a surface is uncomplicated. Bimolecular hopping and lateral interaction between the different sites within the monolayers have been ruled out however, the behaviour of these systems is dependent on the nature of the solvent and electrolyte with greater ion pairing observed between the oxidised redox centre and perchlorate ions from the electrolyte.[14a]

STM images of the $[Os(bipy)_2(p2p)_2]^{2+/3+}$ monolayer on a Au(III) surface show that this system forms a loosely disordered monolayer with areas of ordered domain identified. The electron transfer rates for the Os monolayers (adiabatic) in Figure 3.1 are almost three orders of magnitude greater than that of the Co complex (diabatic limit). *In situ* electrochemical STM studies have shown that a clear tunnelling maximum is observed close to the equilibrium redox potential of the former and the transfer of electrons from the molecule and the enclosing electrodes (substrate and STM tip) has been deemed to be that of a two-step sequential electron transfer process. These results suggest that these types of osmium complexes may be deemed suitable as transistor-like components for the construction of molecular electronic devices.

The electrochemical properties of four mononuclear ruthenium and osmium complexes, of the general formula $[M(bipy)_2L]^{2+}$ where M is either ruthenium or osmium, bipy is 2,2'-bipyridyl and L represents either the ligand 2-(4-pyridyl)imidazole[f]-1,10-phenanthroline or 2-(3-thio)imidazole[f]-1,10-phenanthroline have been studied. These complexes have been synthesised by Laura Cleary, Prof. J.G. Vos research group. Monolayers of all four complexes have been obtained and the complexes have been analysed using cyclic voltammetry, differential pulse voltammetry, resonance Raman spectroscopy and SERS. The molecular structure of each complex is shown in Figure 3.2. For the purpose of discussion the names of each of the complexes have been abbreviated, Table 3.1.

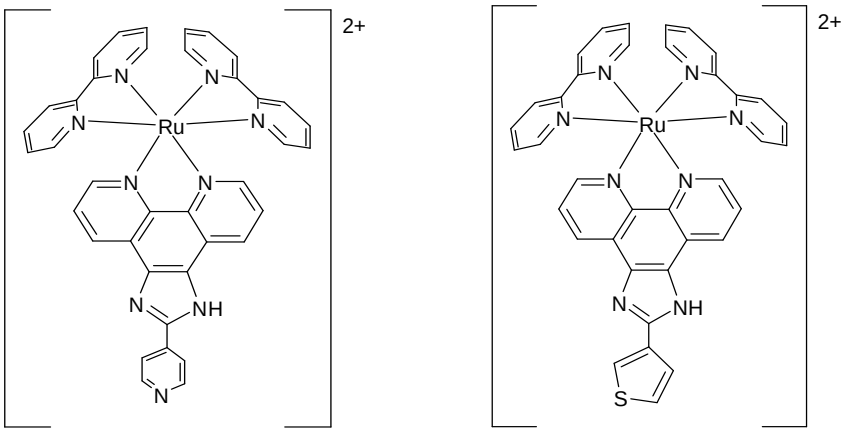

Ru(pyrphen) **Ru(thimphen)**

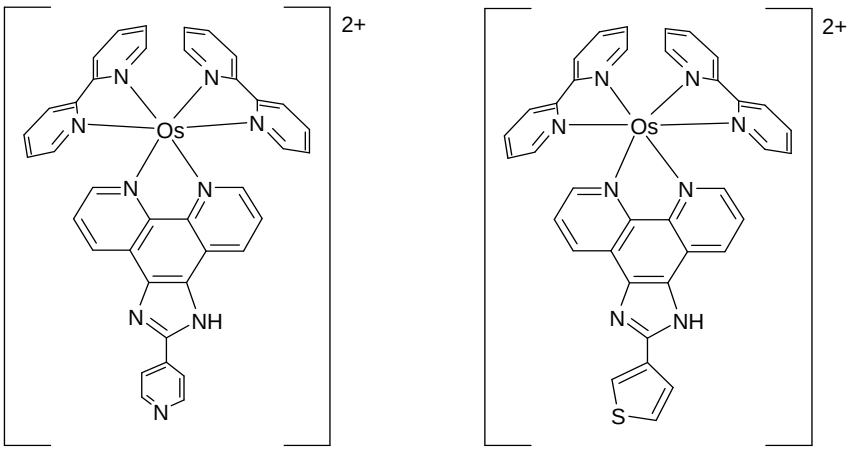

Os(pyrphen) **Os(thimphen)**

Figure 3.2: *Molecular structures of the mononuclear M(pyrphen) and M(thimphen) complexes, where M = Ru/Os .*

Full Name	**Abbreviation**
$[Ru(bipy)_2(2\text{-}(4\text{-pyridyl})imidazole[f]\text{-}1,10\text{-phenanthroline})]^{2+}$	Ru(pyrphen)
$[Ru(bipy)_2(2\text{-}(3\text{-thio})imidazole[f]\text{-}1,10\text{-phenanthroline})]^{2+}$	Ru(thimphen)
$[Os(bipy)_2(2\text{-}(4\text{-pyridyl})imidazole[f]\text{-}1,10\text{-phenanthroline})]^{2+}$	Os(pyrphen)
$[Os(bipy)_2(2\text{-}(3\text{-thio})imidazole[f]\text{-}1,10\text{-phenanthroline})]^{2+}$	Os(thimphen)

Table 3.1: *Abbreviations used to label each of the four ruthenium and osmium complexes.*

3.2 Results and Discussion

3.2.1 Redox Properties

Cyclic voltammetry (CV) and Differential Pulse Voltammetry (DPV) are two electrochemical techniques employed in the characterisation of these complexes. The oxidation potentials for each complex are detailed in Table 3.2. Analysis using cyclic voltammetry reveals a single reversible anodic wave at positive potentials which is observed in the CV of each of the four monomers, Figure 3.3. This is assigned as the oxidation of the metal centre with the removal of an electron according to the following process: $M^{II} \rightarrow M^{III} + e^-$. The theoretical peak to peak separation between the anodic and cathodic waves of a redox process (ΔE_p) for a one electron process is 59 mV at room temperature.[17, 18, 19] However, an experimental range of 60 – 100 mV is generally accepted as a one electron process. Values in the range of 55 – 65 mV were recorded for ΔE_p of each mononuclear complex investigated.

The ruthenium complexes are oxidised at potentials approximately 450 mV more positive than the corresponding osmium analogues. The 4d orbitals house electrons that are higher in energy and hence more polarizable than the electrons of the 5d orbitals in osmium. As a result of this, a stronger driving force (more positive potential) is required to remove an electron from the outer orbitals of the ruthenium complexes.[20]

Comparing the oxidation potentials of the M(pyrphen) and M(thimphen) complexes it is noted that there is very little difference between the two. This would suggest that the coupling between the linker group (pyridine or thiophene) of the phenanthroline-imidazole ligand and the metal centres is weak in these types of mononuclear complexes. Even though the M(pyrphen) complexes are oxidised at slightly higher (more positive) potentials than their M(thimphen) counterparts (due to the stronger electron withdrawing properties of the pyridine ring) a larger difference in potentials between the two would be expected if the coupling was strong.

Complex	***Electrode***	$E_{1/2\ ox.}$ ***(V)***	$E_{pa} - E_{pc}$ ***(mV)***	$E_{1/2\ red.}$ ***(V)***	$E_{pc} - E_{pa}$ ***(mV)***
Ru(pyrphen)	GC	+1.33	60	-1.24 (irr.)	-
				-1.48	65
				-1.73	70
				-2.07	70
				-2.38	110
				-2.64	120
Ru(thimphen)	GC	+1.28	55	-1.37	30
				-1.48	80
				-1.58	60
				-1.98	70
				-2.40	150
				-2.69	120
Os(pyrphen)	GC	+0.89	60	-1.18 (irr.)	-
				-1.41	60
				-1.70	65
				-2.01	80
				-2.35 (irr.)	-
				-2.46 (irr.)	-
Os(thimphen)	GC	+0.86	60	-1.27	30
				-1.42	80
				-1.53	80
				-1.92	60
				-2.30	100
				-2.60	90
$[Ru(bipy)_3]^{2+}$	GC	+1.29	70	-1.33, -1.52, -1.76	60, 65, 65
$[Os(bipy)_3]^{2+}$	Pt	+0.83	-	-1.28	-

Table 3.2: *Electrochemical potentials of the mononuclear complexes (vs. SCE) using 0.1 M $TBAPF_6$ in acetonitrile as the supporting electrolyte. Scan rate: 100 mV/s. GC working electrode (3 mm geometrical diameter). The parent complexes, $[Ru(bipy)_3]^{2+}$ and $[Os(bipy)_3]^{2+}$* [20] *are included for comparison.*

The electrochemistry of two ruthenium derivatives has been reported by Zhou et al. [21] where the pyrphen ligand (2-(4-pyridyl)imidazole[f]-1,10-phenanthroline) ligand is replaced by imidazo[4,5-*f*]1,10-phenanthroline (ip) and 2-phenylimidazo[4,5-*f*][1,10]phenanthroline (pip). The oxidation potentials of the complexes

$[Ru(bipy)_2(ip)]^{2+}$ and $[Ru(bipy)_2(pip)]^{2+}$ are +1.25 and +1.28 V respectively (vs. SCE). The presence of the π-acceptor phenyl ring on the pip ligand decreases the σ-donor properties which results in an anodic shift of 30 mV compared to that of the ip complex. Further π-delocalization results in a stabilisation of the metal d_π orbitals which accounts for the increase in the oxidation potential. Pyridine rings have greater π-acceptor capabilities than phenyl rings pulling even more electron density away from the metal. This may account for the observed increase in the redox potential of Ru(pyrphen) when comparing it to $[Ru(bipy)_2(ip)]^{2+}$ and $[Ru(bipy)_2(pip)]^{2+}$.

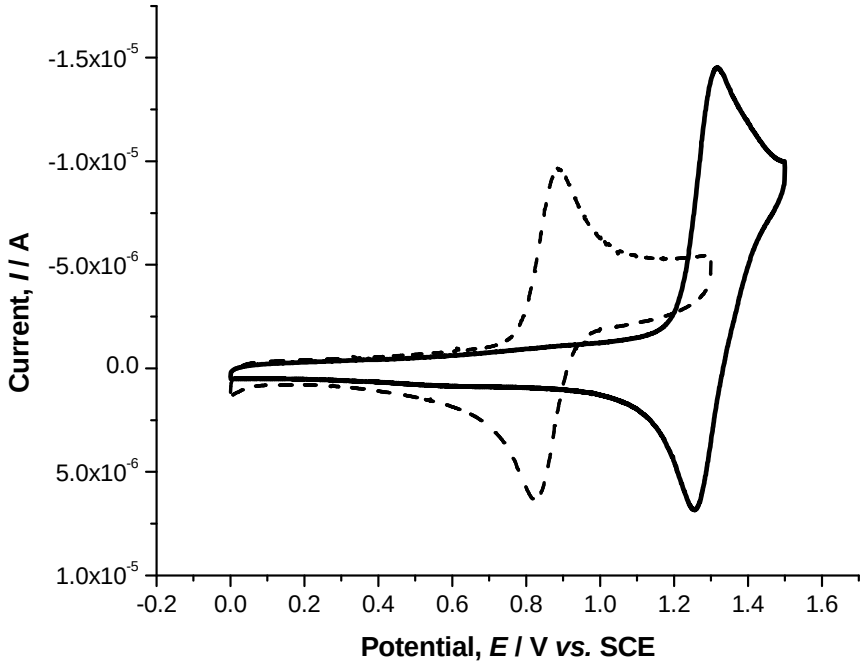

Figure 3.3: *Cyclic voltammetry of Os(thimphen), dashed line, and Ru(thimphen), solid line, at a GC electrode (3 mm geometrical diameter), vs. SCE, using 0.1 M $TBAPF_6$ as the supporting electrolyte. Scan rate: 100 mV/s.*

Using a glassy carbon working electrode, in acetonitrile based electrolyte, a potential window with a negative limit of -2.9 V has been achieved. Within this window several cathodic processes have been observed. Under anaerobic conditions, up to six reductive waves are present in the cyclic voltammogram of Ru(pyrphen) in acetonitrile, Figure 3.4. The first (least negative) of these peaks occurs at a potential of -1.24 V (*vs.* SCE) and is irreversible at slow scan rates, *vide infra*. This wave is also

present for the osmium analogue but it does not appear in the cyclic voltammograms of either of the thimphen derivatives. Based on this result alone it would appear that this reduction is associated with the phenanthroline – pyridine ligand where an electron is added to a π^* orbital on this highly conjugated planar ligand. Cooke *et al.* [22] reported reduction potentials for a similar compound, $[Ru(bipy)_2(phen)]^{2+}$ (where phen is 1,10-phenanthroline). The first ligand reduction of this complex was compared to that of the corresponding reduction in $[Ru(bipy)_3]^{2+}$ with reported potentials of -1.33 and -1.34 V (*vs.* SCE) respectively. This suggests that the addition of the imidazole-pyridine/thiophene moiety to the phenanthroline ligand is responsible for altering the energy of the LUMO level, with respect to that of bipyridine, in each compound.

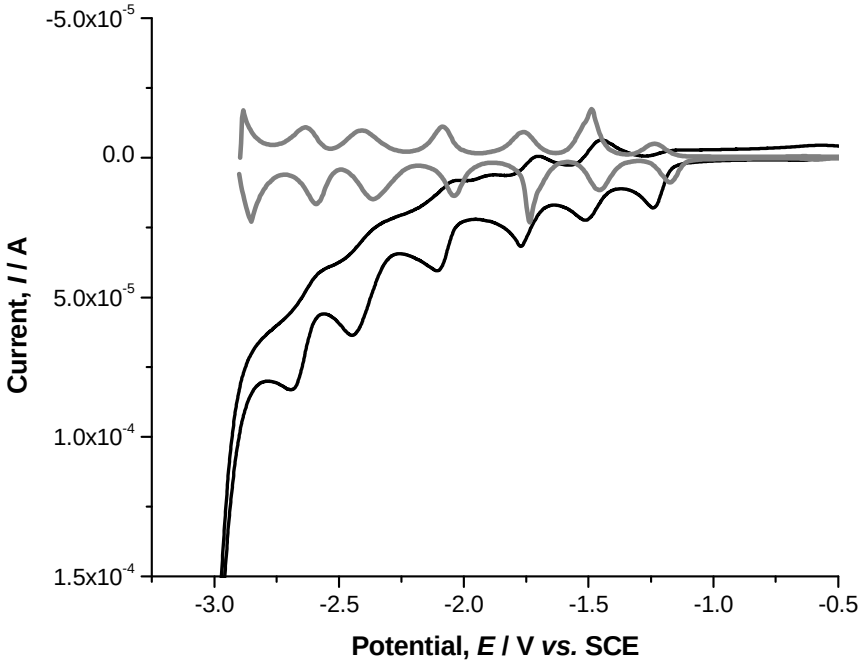

Figure 3.4: *Cyclic voltammetry (black line) and differential pulse voltammetry (grey line) of the reductions of Ru(pyrphen) at a GC electrode (3 mm geometrical diameter), vs. SCE, using 0.1 M $TBAPF_6$ in acetonitrile. Scan rate: 100 mV/s.*

By comparison of the reduction potentials of Ru(pyrphen) with those of the parent complex, $[Ru(bipy)_3]^{2+}$ (Table 3.2) it is noted that the first reduction potential of $[Ru(bipy)_3]^{2+}$ is seen at -1.35 V which is almost 100 mV more negative than this first

process in Ru(pyrphen). Reductive spectroelectrochemistry supports this proposal that the LUMO of the pyrphen complexes is actually located on the pyrphen ligand itself, however, excited state Raman spectroscopy indicates that the lowest lying π* orbital involved in the excited state chemistry of this complex is not in the same location as the LUMO, *vide infra*.

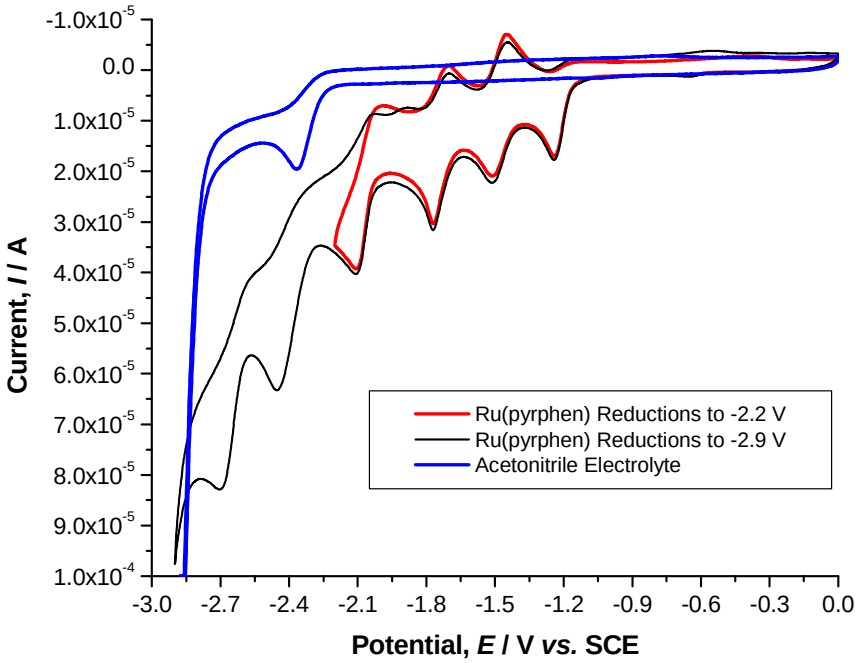

Figure 3.5: *Cyclic voltammetry of the reductions of Ru(pyrphen) (black and red lines) at a GC electrode (3 mm geometrical diameter), vs. SCE, using 0.1 M TBAPF$_6$ in acetonitrile. The CV of the blank electrolyte is included (blue line). Scan rate: 100 mV/s.*

The second and third cathodic processes have reduction potentials within the region of the second and third reductions recorded for $[Ru(bipy)_3]^{2+}$, Table 3.2, and as a result are assigned as bipyridyl based reductions. A further three cathodic waves are observed with cathodic peak potentials of -2.11, -2.45 and -2.71 V, Figure 3.4, and these processes are not fully reversible. When compared with the blank electrolyte (0.1 M $TBAPF_6$ in acetonitrile) it was found that the cathodic wave at -2.45 V is also present in the CV of the blank electrolyte (E_{pc} = -2.37 V), Figure 3.5. Cryogenic

temperatures are required for the addition of a second electron to the bipy anion radical created upon reduction of the bipy ligand.[23] Taking this into account, along with the observation that the two reductions at -2.11 and -2.71 V are not observed in the CV of the blank electrolyte, these processes have been assigned as being located on the pyrphen ligand.

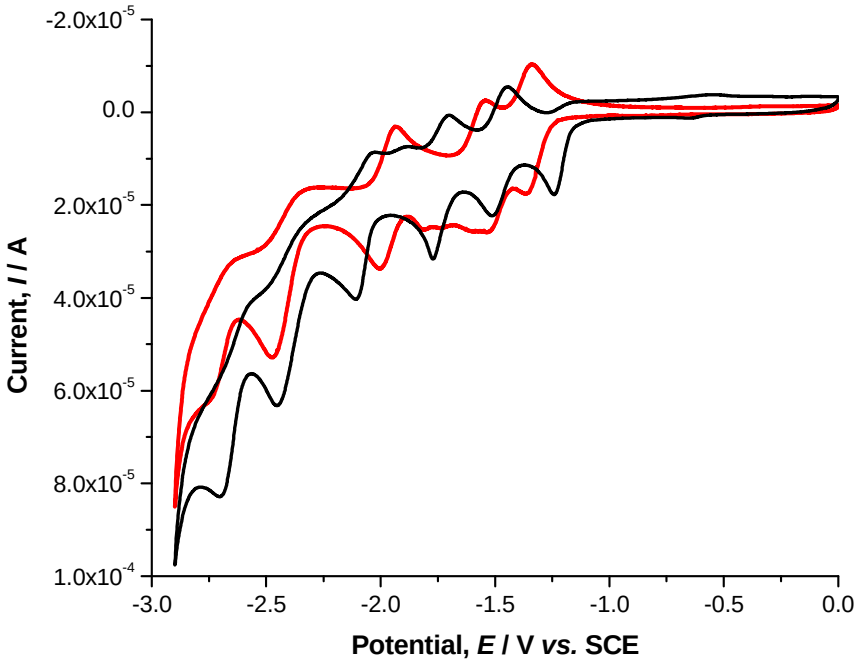

Figure 3.6: *Cyclic voltammetry of the reductions of Ru(pyrphen) (black line) and Ru(thimphen) (red line) at a GC electrode (3 mm geometrical diameter), vs. SCE, using 0.1 M TBAPF$_6$ in acetonitrile. Scan rate: 100 mV/s.*

The reductive electrochemistry of Ru(thimphen) reveals five well defined cathodic processes within a potential window of 0 to -2.9 V, Figure 3.6. The first (least negative) and second well defined reversible reduction peaks have half-wave potentials of -1.37 and –1.54 V (Table 3.2). These processes have been assigned as bipyridyl based ligand reductions by comparison with $[Ru(bipy)_3]^{2+}$. There are additional processes occurring (-1.9 > E_{pc} > -1.5 V) that are of very weak intensity which may be a product of adsorptive processes on the electrode surface in acetonitrile. Scanning to more negative potentials reveals a third reversible process as well as additional cathodic peaks which, like those observed for Ru(pyrphen), are not

fully reversible. The wave at -2.47 V has been assigned as that of the reduction of the solvent with the remaining cathodic waves associated with the thimphen ligand.

Complex	$E_{1/2\ ox.}$ **(V), vs. SCE**	$E_{1/2\ red.}$ **(V)**
Ru(pyrphen) **RT**, *acetonitrile*	+1.33	-1.24 (E_{pc}), -1.48, -1.73
Ru(pyrphen) **RT**, *dichloromethane*	+1.19 (E_{pa})	-1.48 (E_{pc} = -1.54), -1.72, -1.96
Ru(pyrphen) **LT**, *dichloromethane*	+1.13 (E_{pa} = +1.20)	-1.60 (E_{pc}), -1.80, -2.13
Ru(thimphen) **RT**, *acetonitrile*	+1.28	-1.37, -1.58, -1.98
Ru(thimphen) **RT**, *dichloromethane*	+1.21 (E_{pa})	-1.50, -1.84
Ru(thimphen) **LT**, *dichloromethane*	+1.11 (E_{pa} = +1.22)	-1.58, -1.85

Table 3.3: *Redox data for Ru(pyrphen) and Ru(thimphen) at a GC working electrode (3mm geometrical diameter), vs. SCE, in acetonitrile and dichloromethane with 0.1 M $TBAPF_6$ electrolyte. RT = room temperature and LT = low temperature (-70ºC). Scan rate: 100 mV/s.*

Oxidation of the ruthenium mononuclear complexes in dichloromethane, using a glassy carbon working electrode, results in adsorption on the electrode surface. Dichloromethane is an apolar solvent with a polarity of 3.1. Increasing the charge on the complex will result in the oxidised species falling out of solvent and adsorbing on the electrode surface. This is not observed in acetonitrile as this is a solvent of stronger polarity than dichloromethane.[24] The oxidation potentials recorded for the ruthenium complexes in dichloromethane are less positive than those recorded when acetonitrile is used in the electrolyte system, Table 3.3. When comparing the oxidation potentials of both ruthenium complexes in the different solvents it is noted that they shift toward more negative potentials when dichloromethane is used as the electrochemical solvent. This same observation has been made for the reduction potentials of each complex, Table 3.3. The potential window obtained within

dichloromethane is narrower than that achieved with acetonitrile. As a result not all of the cathodic processes that are visible in the latter appear in dichloromethane, Figure 3.7.

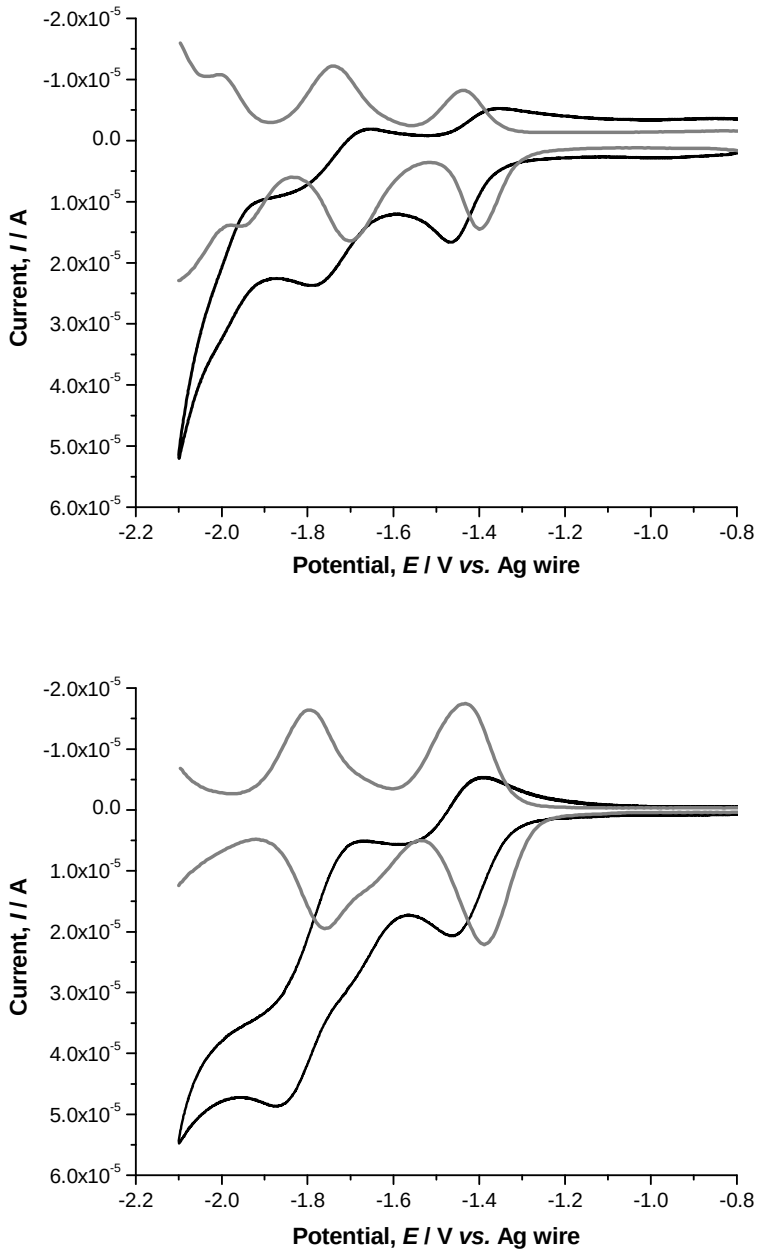

Figure 3.7: *Cyclic voltammetry of the cathodic processes of Ru(pyrphen) (top) and Ru(thimphen) (bottom), at a GC electrode (3 mm geometrical diameter), vs. Ag wire, using 0.1 M $TBAPF_6$ in dichloromethane at room temperature. Scan rate: 100 mV/s.*

The intensity of the return wave of the first reduction of Ru(pyrphen) appears to increase in dichloromethane compared to the corresponding peak in acetonitrile. This process is also associated with the Os(pyrphen) complex and not observed with the M(thimphen) complexes. This observation suggests that this process involves the pyridine ring of the pyrphen ligand. When the pyrphen ligand is reduced the extra electron density and decreased overall charge of the molecule leaves the pyridine ring susceptible to protonation. The presence of water in acetonitrile may provide the proton source for this protonation whereas dichloromethane is only sparingly soluble in water and this may reduce the chance of this process occurring when dichloromethane is used as the electrochemical solvent.

In cases where the return wave of a redox peak is not observed the process may be deemed irreversible. This irreversibility can result for a couple of different reasons. The first of these is that the kinetics of the back reaction is slow and the redox process is incomplete within the time frame of the cyclic voltammetric cycle. Alternatively, following the initial forward reaction at the electrode, a proceeding chemical reaction may occur involving the redox intermediate and preventing the back reaction from taking place.[19] A possible explanation for the irreversibility of the first cathodic process of Ru(pyrphen) may be that the pyridine ring is protonated upon addition of an electron via an electrochemical – chemical (EC) mechanism.

Increasing the scan rate, ν, in cyclic voltammetry allows for the investigation of the true nature of the back reaction of a redox process: can increasing the scan rate allow for the back reaction to occur by outrunning the proceeding chemical reaction of the oxidised or reduced species?

Figure 3.8 includes the cyclic voltammetry of Os(pyrphen) at a Pt macro electrode. The potential window was sufficiently narrow to only allow for the first reduction to occur. As the scan rate increased the intensity of the corresponding anodic wave also increased, Figure 3.9. The increasing IR drop between the working and reference electrodes is evident in Figure 3.8 where the cathodic peak potential shifts slightly in the negative direction with increasing scan rate. This effect is not as pronounced with the use of Au micro electrodes as the working electrode however noise is observed in the CV at scan rates of 40 V/s and higher.

With cyclic voltammetry, as the potential is swept from the initial to the final potential the reactant within the diffusion layer at the electrode surface undergoes an electrochemical reaction and will be oxidised or reduced depending on the potential applied. With the case of the M(pyrphen) complexes the first ligand reduction appears irreversible at slow scan rates. At the electrode-solution interface the layer of M(pyrphen) is reduced when a sufficient potential is applied (~ -1.25 V, *vs.* SCE) and a peak is observed in the CV, the current of which reduces as the amount of unreduced reactant decreases. At slow scan rates the timescale for the proposed proceeding chemical reaction (possibly the protonation of the pyridine) is less than the timescale of the sweep cycle. However, moving to higher scan rates reduces the cyclic voltammetric sweep time and a percentage of the reduced species within the double layer is converted back to the original state as observed through an increase in the intensity of the return wave signifying the corresponding oxidation of the reduced ligand, Figure 3.8 and Figure 3.9. This suggests that this process is in fact a quasi-reversible process and is dependent on the scan rate applied.

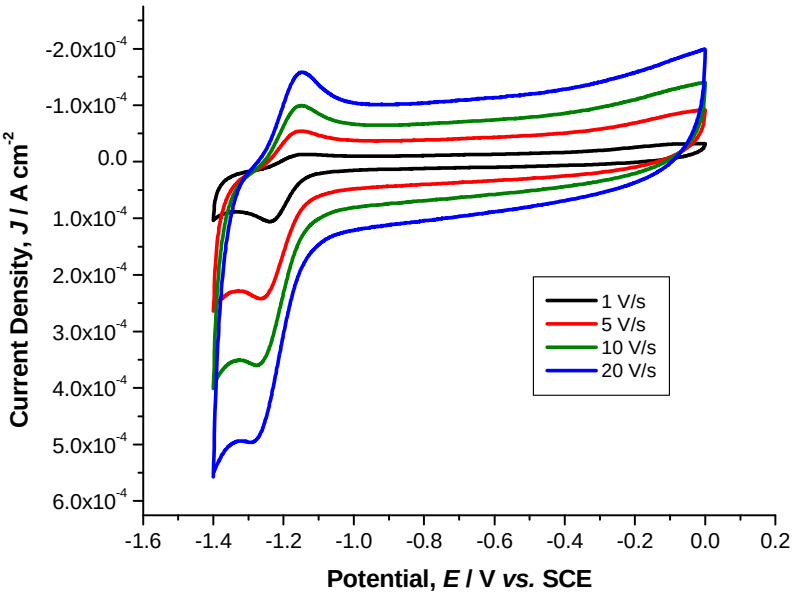

Figure 3.8: *Scan rate dependence of the first reduction process of Os(pyrphen) at a Pt macro electrode using 0.1 M $TBAPF_6$ in acetonitrile as the working electrolyte.*

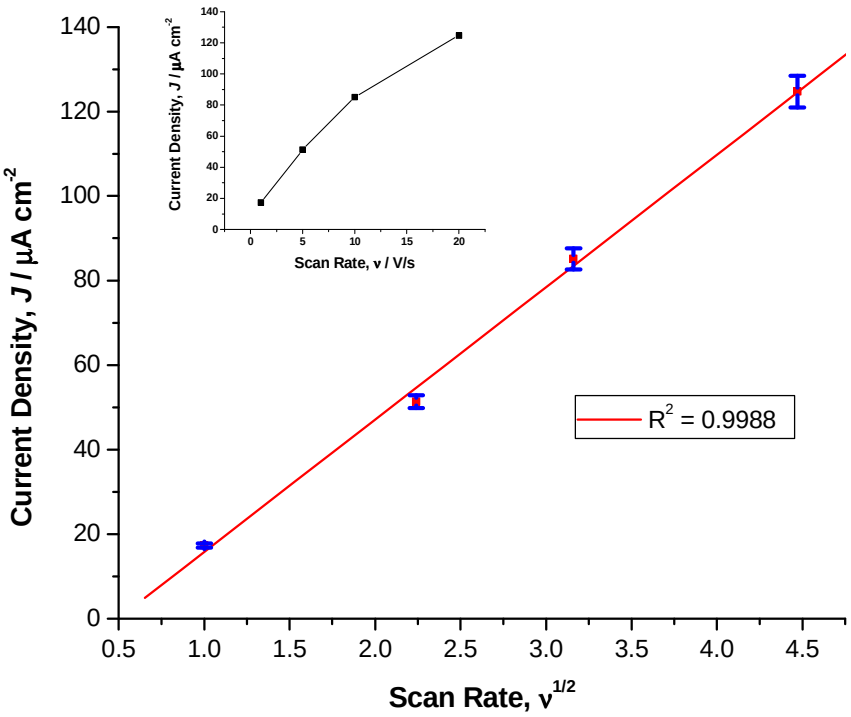

Figure 3.9: *Graph to illustrate the relationship between the current density, J, of the first cathodic process, with the square root of the scan rate, $v^{1/2}$, and J vs. v (inset), for Os(pyrphen) at a Pt macro electrode.*

The electrochemistry of each ruthenium mononuclear complex was investigated at low temperatures (T = ~-80º C) using cyclic voltammetry and differential pulse voltammetry, Figure 3.10 to Figure 3.12. At such low temperatures, the electroactive species should diffuse away from the electrode surface at slower rates than would occur at room temperature. Therefore by carrying out low temperature experiments the possibility of diffusion being the limiting factor in determining the reversibility of the first ligand reduction of Ru(pyrphen) could be considered. A mixture of ethyl acetate and liquid nitrogen was used to obtain temperatures as low as approximately -80º C.[25] As a result of this low temperature acetonitrile, could not be used as the electrochemical solvent as it has a freezing point of ~ -44º C.[25] Dichloromethane, which has a freezing point of ~ -95º C [26], was used instead.

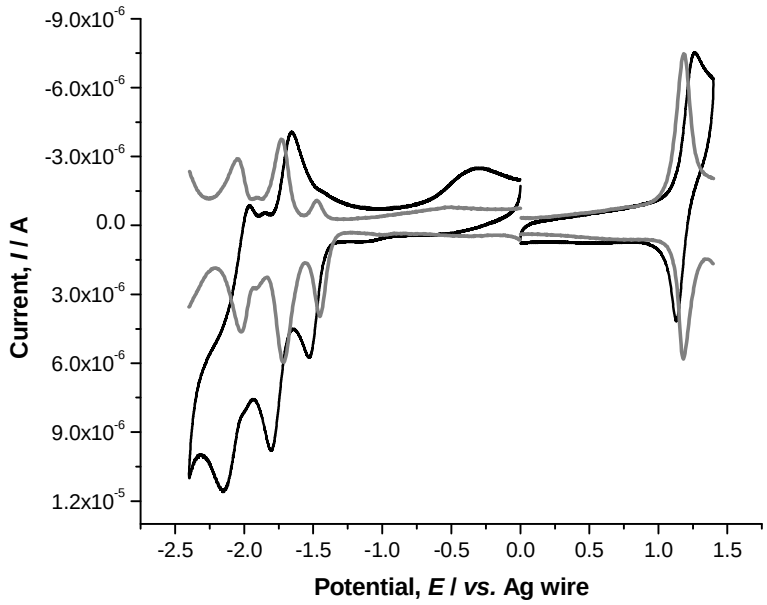

Figure 3.10: *Cyclic voltammetry (black line) and differential pulse voltammetry (grey line) of Ru(pyrphen), at a GC electrode (3 mm geometrical diameter), vs. Ag wire, using 0.1 M $TBAPF_6$ in dichloromethane (temperature ~ -80º C). Scan rate: 100 mV/s.*

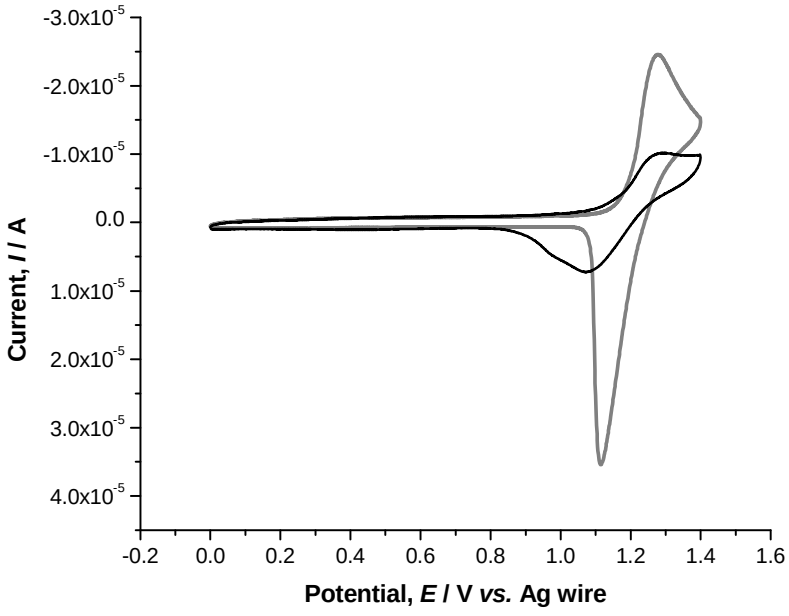

Figure 3.11: *Cyclic voltammetry of the oxidation of Ru(thimphen) at room temperature (grey line) and ~ -80º C (black line),), at a GC electrode (3 mm geometrical diameter), vs. Ag wire, using 0.1 M $TBAPF_6$ in dichloromethane as the supporting electrolyte. Scan rate: 100 mV/s.*

Comparing the oxidation and reduction potentials of each complex in dichloromethane at both room temperature and low temperature (Table 3.3) it is noted that the oxidation of the metal centre is not heavily affected by the change in temperature. A difference of 10 mV, between the two temperatures, in the oxidation potential of each metal complex is observed which is within the range of experimental error. The effect of adsorption of the oxidised species on the glassy carbon electrode surface is reduced at lower temperatures as observed in Figure 3.11. However, the distance between the anodic and cathodic peak potentials, ΔE_p, is increased at temperatures of approximately -80º C which is possibly due to the effect on the heterogeneous electron transfer kinetics.

At -80º C, Figure 3.12, the potential window of dichloromethane is extended to -2.4 V. The third reduction of the Ru(pyrphen) which, at room temperature has a peak potential on the cusp of the end of the solvent potential and as a result is not well defined, is observed clearly at low temperatures. The cathodic peak potential of the first ligand reduction of this complex is shifted by approximately 60 mV toward more negative potentials at low temperature. The intensity of the corresponding return wave is also reduced compared to that observed at room temperature in dichloromethane. The diffusion of a species from the electrode surface into the bulk solution can change dramatically with changes in temperature. At room temperature, the diffusion of an analyte through a solution exhibits Arrhenius type behaviour. The rate constant of reactions are also heavily dependent on solution temperature. According to the Arrhenius equation the rate constant, ln *k* is inversely proportional to the temperature according to the following expression:

Equation 3.1 $$k = \mathrm{A}e^{-Ea/RT}$$

It would be expected therefore that the diffusion of the reduced Ru(pyrphen) complex would occur at a slower rate at low temperatures. A possible explanation for the irreversibility of this first reductive process may be that it is dependent on the rate of diffusion of the reduced complex. Cycling at -80º C should decrease the rate of diffusion. If the probability of the re-oxidation of the reduced ligand of Ru(pyrphen), occurring within the timeframe of the voltammetric cycle is dependent on diffusion

then the intensity of the return wave would be expected to increase at such low temperatures compared to that observed at room temperature. However, this is not observed and therefore it is proposed that the quasi-reversibility of this first cathodic process in Ru(pyrphen) is as a result of a proceeding chemical reaction which may be out-run by increasing the scan rate.

The reductive electrochemistry of the second mononuclear ruthenium complex, Ru(thimphen), was also studied at -80º C in dichloromethane, Figure 3.12. The main difference observed between the electrochemistry in dichloromethane at room temperature and at -80º C is that the first (least negative) cathodic process, which is proposed to be located on a bipyridyl ligand in the M(thimphen) complexes, is shifted by approximately 80 mV in the negative direction. The peak potentials of the subsequent reductions as well as the oxidation potential of the metal centre at -80º C are the same as those observed at room temperature within experimental error, Table 3.3.

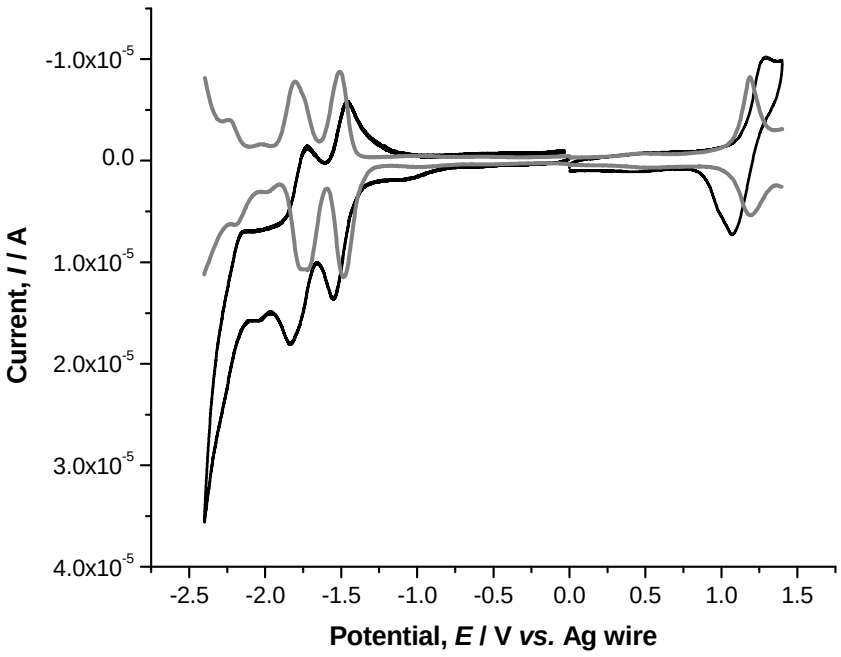

Figure 3.12: *Cyclic voltammetry (black line) and differential pulse voltammetry (grey line) of Ru(thimphen), at a GC electrode (3 mm geometrical diameter), vs. Ag wire, using 0.1 M $TBAPF_6$ in dichloromethane at -80º C. Scan rate: 100 mV/s.*

3.2.2 Spectroelectrochemistry – Oxidative

Spectroelectrochemistry is an analytical technique that incorporates electrochemistry with spectroscopy to analyse both organic and inorganic compounds. Each of the four transition metal complexes discussed in this chapter have been analysed using both oxidative and reductive spectroelectrochemistry. This consists of electrochemically generating the oxidised or reduced form of each complex and studying the associated changes in the electronic absorption spectra. A more detailed introduction into spectroelectrochemistry is given in Chapter 4. Chapter 4 focuses on dinuclear complexes and the use of spectroelectrochemistry to assign redox processes to specific metal centres while investigating the interaction between them. This chapter looks at using spectroelectrochemistry as an accompanying technique to cyclic voltammetry in the assignment of the redox processes in each of the four complexes.

In contrast to Os^{II} complexes, where ^{1}MLCT and ^{3}MLCT absorbance bands are observed, only ^{1}MLCT absorbance bands are observed in Ru^{II} complexes, Figure 3.13.

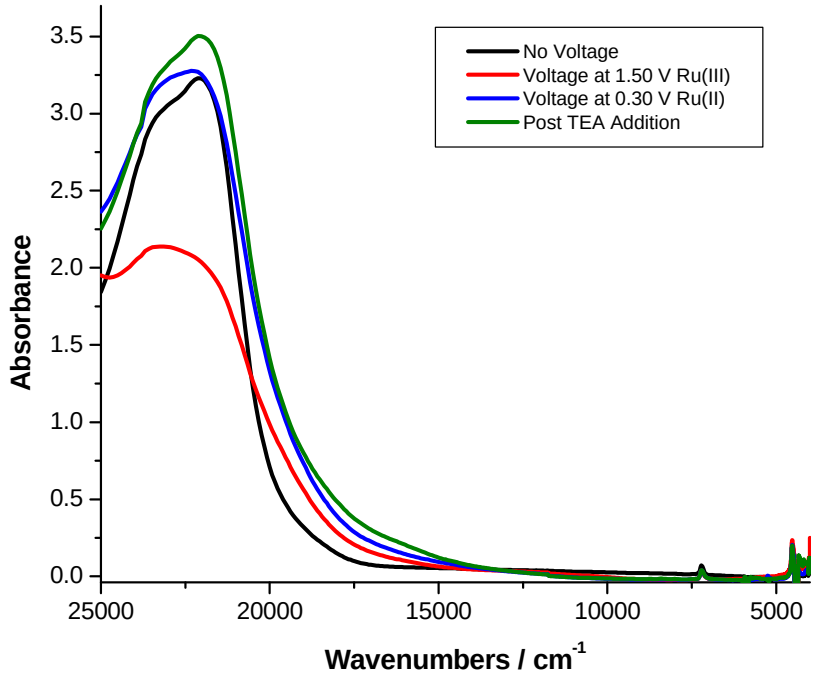

Figure 3.13: *Spectroelectrochemistry of Ru(pyrphen) using a Pt gauze working electrode, vs. SCE, using 0.1 M $TBAPF_6$ in acetonitrile as the supporting electrolyte.*

The importance of spin-orbit coupling (which can be defined as the mixing of the molecules spin angular momentum with the orbital angular momentum) increases down a group in the d-block of elements in the periodic table from light to heavier atoms (e.g., Fe → Ru → Os →...). Such formally spin-forbidden transitions as ^{3}MLCT – the transfer of charge from the dπ metal centred orbitals to the π* orbitals centred upon the ligands – are observed in the absorbance spectra of osmium complexes but these bands are a lot weaker and not often observed in the spectra of ruthenium complexes.[20]

The absorbance spectrum of Ru(pyrphen), Figure 3.13, reveals ^{1}MLCT bands in the region of 25000 – 20000 cm^{-1} (400 -500 nm). Upon oxidation by bulk electrolysis (potential held at +1.50 V, $E_{½}$ = +1.31 V, *vs.* SCE) the intensity of these absorbance bands decreases due to the lessening of t_{2g} back-bonding from the Ru^{III} metal to the ligand π* orbitals. When the solution of Ru(pyrphen) is fully oxidised a very weak broad absorption is observed, 16700 – 10000 cm^{-1} (600 – 1000 nm), which may be assigned as an LMCT absorption band of the transfer of electron density from the ligand to the oxidised Ru^{III} metal centre. This signal is no longer observed when the complex is reduced back to Ru^{II} state.

Upon investigation of the re-reduced species (potential held at +0.30 V) it was noted that although the intensity of the ^{1}MLCT bands returned back to the original state the shape of the peak did not. A possible explanation for this is that the complex may have been protonated with the nitrogen atom on the pyridine ring offering a protonation site. Water is oxidised above +1.0 V which produces H^+ ions which can result in an increase in the acidity of the solution. Any water that entered the system during the experiment could have resulted in protonation. Addition of the base, tetraethyl ammonium (TEA), resulted in an absorbance spectrum with ^{1}MLCT bands of the same intensity and shape as the original MLCT band of the Ru^{II} complex prior to oxidation. The intensity of these absorbance bands, following addition of the base is, however greater than the original spectrum. This may be due to evaporation of solvent over the time taken to carry out the experiment.

The spectroelectrochemistry of Ru(thimphen) is quite similar to that of Ru(pyrphen) in that, prior to oxidation, ^{1}MLCT absorbance bands are observed in the region of

25000 – 19200 cm^{-1} (400 – 520 nm), Figure 3.14. The $E_{1/2}$ of Ru(thimphen) is +1.30 V, *vs.* SCE (Table 3.2) . To oxidise the entire solution of the complex within the cell the potential was held at +1.40 V (*vs.* SCE) via bulk electrolysis. The intensity of the ^{1}MLCT bands decreases upon oxidation of the metal centre and a low intensity, broad LMCT band is revealed from 18200 – 12500 cm^{-1} (550 – 800 nm) which is not present in the spectrum of the re-reduced complex.

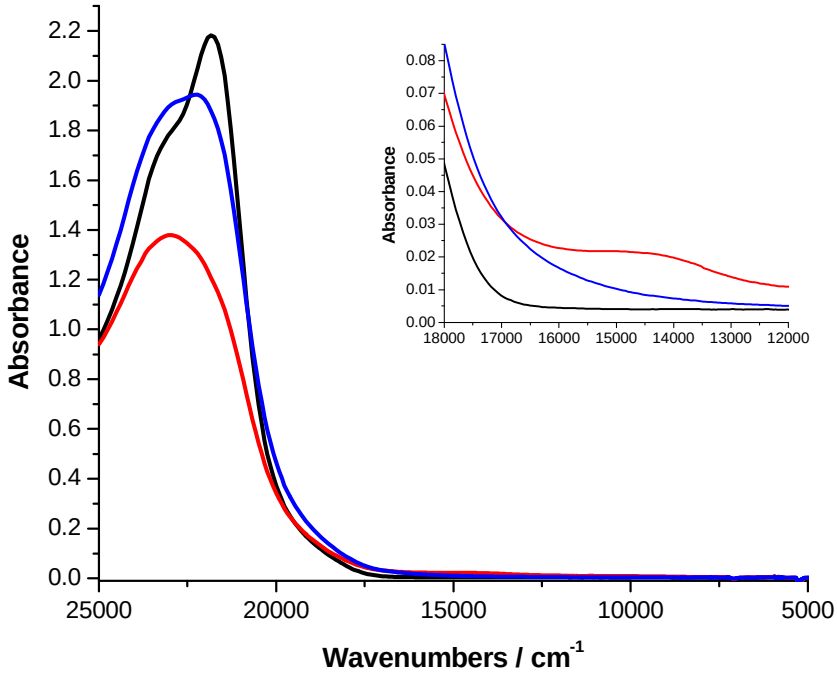

Figure 3.14: *Spectroelectrochemistry of Ru(thimphen) using a Pt gauze working electrode, vs. SCE, using 0.1 M $TBAPF_6$ in acetonitrile as the supporting electrolyte. The black line represents the spectrum of the complex prior to the applied potential. The red and blue lines indicate the oxidised and re-reduced spectra respectively. Inset: LMCT bands in the region of 18000 – 12000 cm^{-1}.*

Upon bulk reduction (potential held at +0.30 V) of the system it was discovered that the oxidation was not fully reversible. This irreversibility of the process involving the oxidation to Ru^{III} implies that a change in the distribution of electron density within the complex has occurred. This would lead to a change in the shape of the ^{1}MLCT. It is not fully known where the change in the distribution of electron density occurs on the complex. However, the possibility of electropolymerisation of the thiophene rings

has been ruled as a much greater change in the absorbance spectra would be expected if the complex was polymerising on the surface of the electrode.[27]

In contrast to ruthenium complexes, both ^{1}MLCT and ^{3}MLCT absorption bands are observed in the spectra of osmium complexes in the 2+ oxidation state (i.e. Os^{II}). These are observed in the spectra of Os(pyrphen) and Os(thimphen) in the region of 25000 – 13900 cm^{-1} (400 – 720 nm), Figure 3.15. The half-wave potential of Os(pyrphen), $E_{1/2}$ = +0.86, *vs.* SCE, is only 30 mV more positive than that of Os(thimphen) with a half-wave potential of +0.83 V, *vs.* SCE, Table 3.2.

The spectroelectrochemistry of Os(pyrphen) is quite similar to that of the thimphen analogue with the disappearance of the ^{1}MLCT and ^{3}MLCT bands upon oxidation by bulk electrolysis (potential held at +1.20 V, *vs.* SCE), Figure 3.15, confirming that this anodic process is associated with the removal of an electron from the osmium metal centre. The shape and intensity of these absorbance bands return to that of the original spectra when the complex is reduced (potential held at +0.30 V, *vs.* SCE). This indicates that the oxidation of this complex is a reversible process.

The half-wave potential ($E_{1/2}$) of Os(thimphen) is +0.83 V, *vs.* SCE. To ensure the complex was fully oxidised the working electrode was held at a potential of +1.10 V and the scan was repeated five times to ensure the sample was converted fully to the +3 state i.e. Os^{III}. The ^{1}MLCT and ^{3}MLCT absorption bands at 25000 – 18900 cm^{-1} (400 – 530 nm) and 18200 – 13900 cm^{-1} (550-720 nm) respectively, are not observed when the system is fully oxidised.

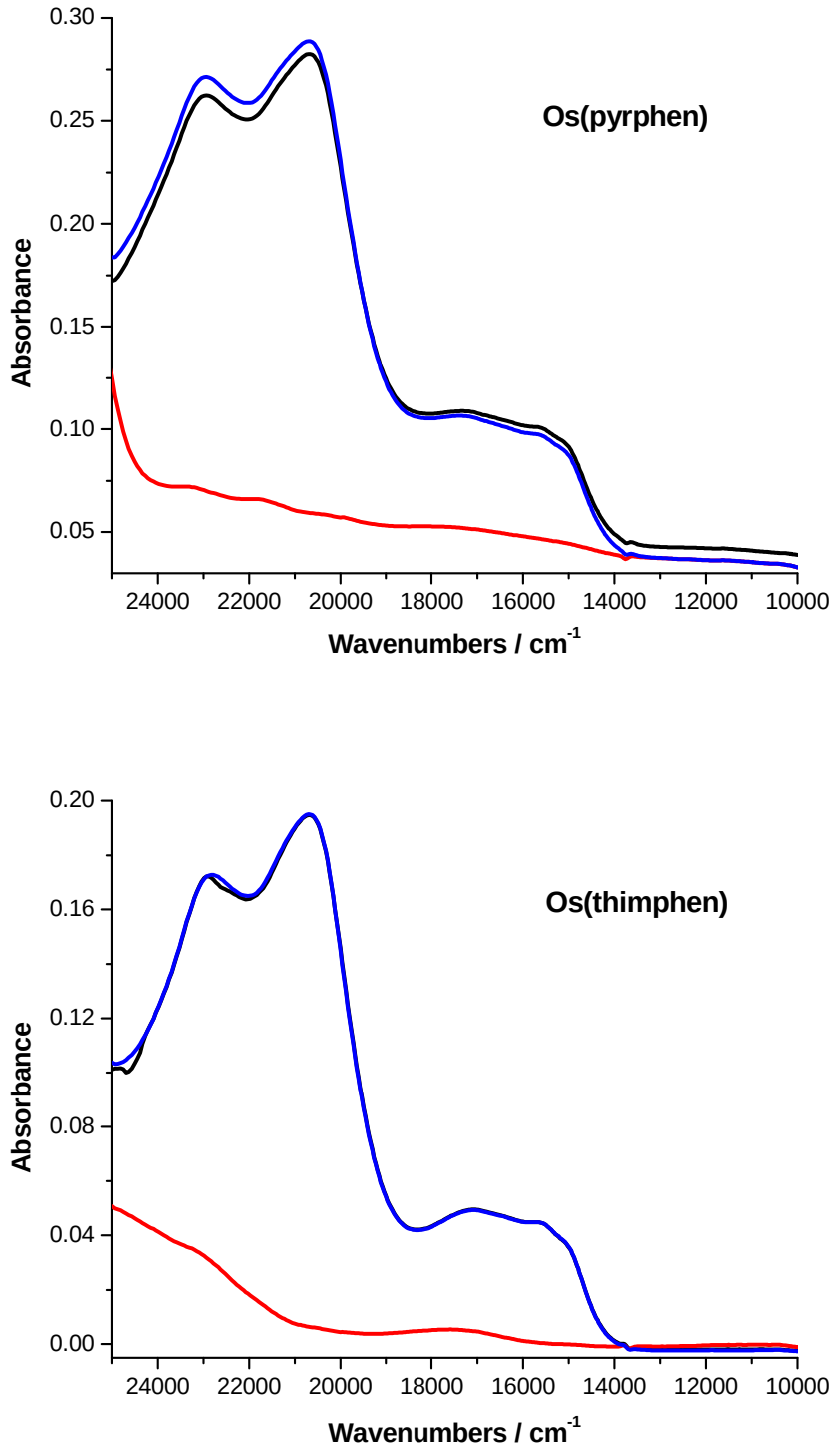

Figure 3.15: *Spectroelectrochemistry of Os(pyrphen) (top) and Os(thimphen) (bottom) using a Pt gauze working electrode, vs. SCE, using 0.1 M $TBAPF_6$ in acetonitrile as the supporting electrolyte. The black line indicates represents the spectrum of the complex prior to the applied potential. The red and blue lines indicate the oxidised and reduced spectra respectively.*

As the complex is re-reduced (+0.30 V, *vs.* SCE) the absorption bands that were observed prior to oxidation are again present in the spectrum indicating the reversibility of this anodic process in Os(thimphen), Figure 3.15. There is a broad, weak absorbance band present at ~11000 cm^{-1} (900 nm), Figure 3.16. This is assigned as an LMCT band of the $Os^{III}(bpy)_2$ part of the molecule as bipyridyl ligands are strong π-acceptor ligands and therefore lead to weak high energy absorbance bands in the UV-Vis spectrum.

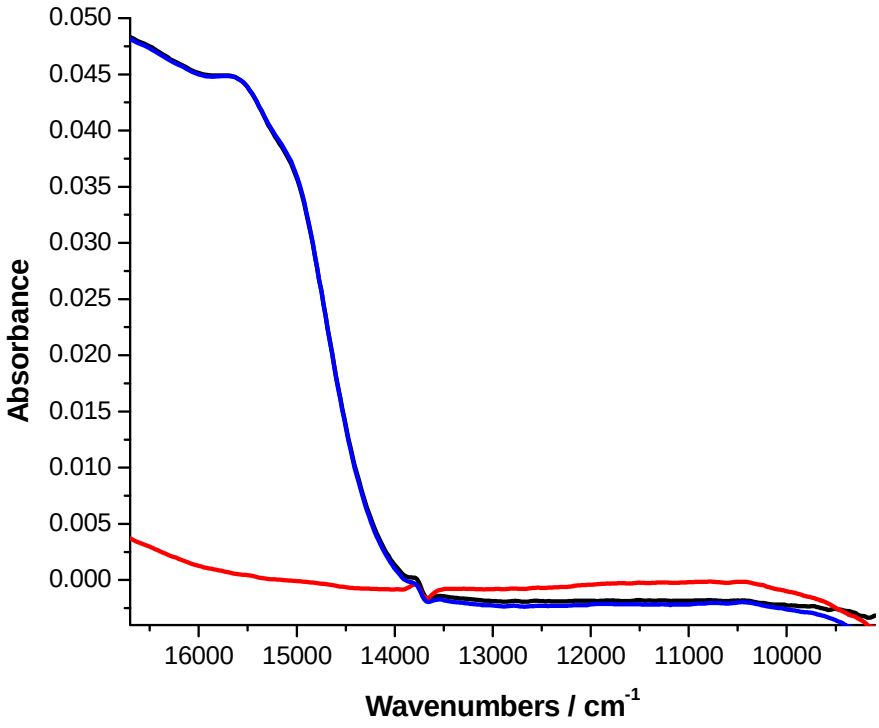

Figure 3.16: *Spectroelectrochemistry of Os(thimphen), focusing on the region 16700-9100 cm^{-1}, using a Pt gauze working electrode, vs. SCE, using 0.1 M $TBAPF_6$ in acetonitrile as the supporting electrolyte. The black line represents the spectrum of the complex prior to the applied potential. The red and blue lines indicate the oxidised and reduced spectra respectively.*

3.2.3 Spectroelectrochemistry – Reductive

In section 3.2.1 the reductive diffusion controlled electrochemistry of this series of ruthenium and osmium mononuclear complexes is discussed. From the analysis of the electrochemistry in several solvents and at several scan rates, it is proposed that the location of the LUMO (and hence the first reduction) differs between the pyrphen and thimphen complexes. Given that the first reduction on the M(pyrphen) complexes is irreversible at slow scan rates, Figure 3.8, and occurs at a potential less negative than that of the first reduction of the parent complex, $[Ru(bipy)_3]^{2+}$ it is proposed that this process is associated with the pyrphen ligand itself. The M(thimphen) complexes however exhibit a first reduction with a potential similar to that of $[Ru(bipy)_3]^{2+}$ and this process is assigned as being a reduction centred on a bipyridyl ligand. Reductive spectroelectrochemistry has been employed to differentiate between the first reductive process of the pyrphen and thimphen complexes.

The reductive spectroelectrochemistry was carried out under an argon atmosphere. The complete exclusion of oxygen is required when scanning to such negative potentials as the reduction of oxygen to superoxide, $O_2^{\cdot -}$ can interfere with the electrochemistry of the analyte in the cell. In slightly basic conditions in acetonitrile the reduction of diatomic oxygen to superoxide can occur at relatively low over potentials, Equation 3.2.

Equation 3.2 $O_2 + e^- \leftrightarrow O_2^{\cdot -}$ (-0.47 V, *vs.* NHE [18])

Bulk electrolysis, at potentials sufficient to achieve the first reduction of the osmium monomers was carried out to generate the singly charged complexes, $[Os(bipy)_2(L)]^+$, where L = thimphen/pyrphen. The appearance of new absorbance bands indicative of the bipy anion radical was used as an indicator for the location of the first cathodic process on each complex. Os(thimphen) was reduced at -1.5 V (*vs.* Ag wire) in order to monitor the changes in the absorbance spectra that were induced by the presence of the $[Os(thimphen)]^+$ complex. These changes are compared with the corresponding spectra of $[Ru(bipy)_3]^+$, Table 3.4.[28]

Complex	$\pi \rightarrow \pi^*$ (bipy) nm	$\pi \rightarrow \pi^*$ (bipy)$^-$ nm	$\pi \rightarrow \pi^*$ (bipy)$^-$ nm	$\pi \rightarrow \pi^*$ (bipy)$^-$ nm
$[Ru(bipy)_3]^{+}$ [28]	292	342	502	781
			529	869
				990
$[Os(thimphen)]^+$	296	333	516	700 - 850†
$[Os(pyrphen)]^+$	292	336	511	ND‡

Table 3.4: *Electronic absorbance data of $[Os(thimphen)]^+$ and the singly reduced parent ion, $[Ru(bipy)_3]^+$. † This absorbance appears as a series of large bands of very weak intensity, Figure 3.17. ‡ The low energy absorbance bands observed for $[Os(thimphen)]^+$ (700-850 nm) are not detected (ND) for $[Os(pyrphen)]^+$ as a result of weaker intensity.*

The formation of the $[Os(thimphen)]^+$ complex is manifested by significant changes in the absorbance spectrum compared with that of $[Os(thimphen)]^{2+}$. The intensity of the bipy $\pi \rightarrow \pi^*$ absorbance bands decreases slightly with a bathochromic shift observed also, Figure 3.17. Additional bands appear in the spectrum following the first reduction of the complex which are observed at 333, 516 and between 700 and 850 nm. These bands fall within the range observed for the corresponding process of $[Ru(bipy)_3]^{+}$ [28] (Table 3.4) and are therefore assigned to intraligand bands from the bipy anion radical. This observation supports the proposal that the LUMO of Os(thimphen) is located on one of the bipy ligands as indicated by the first reduction involving a bipy unit.

Changing the potential to -1.9 V allows for the addition of a second electron and the formation of the $[Os(thimphen)]^0$ complex. This is manifested in the absorbance spectrum by a significant decrease in the intensity of the bipy $\pi \rightarrow \pi^*$ absorbance bands with a concomitant further growth of the bipy anion radical $\pi \rightarrow \pi^*$ bands at 333, 516 and 700 – 850 nm. Bulk electrolysis at 0 V (*vs.* Ag wire) confirms the reversibility of these cathodic processes. The shape of each of the absorbance bands in the spectrum returns to those observed for the $Os(thimphen)^{2+}$ complex prior to reduction. However, the overall intensity has increased due to the evaporation of the solvent as a result of purging with argon over the course of the experiment.

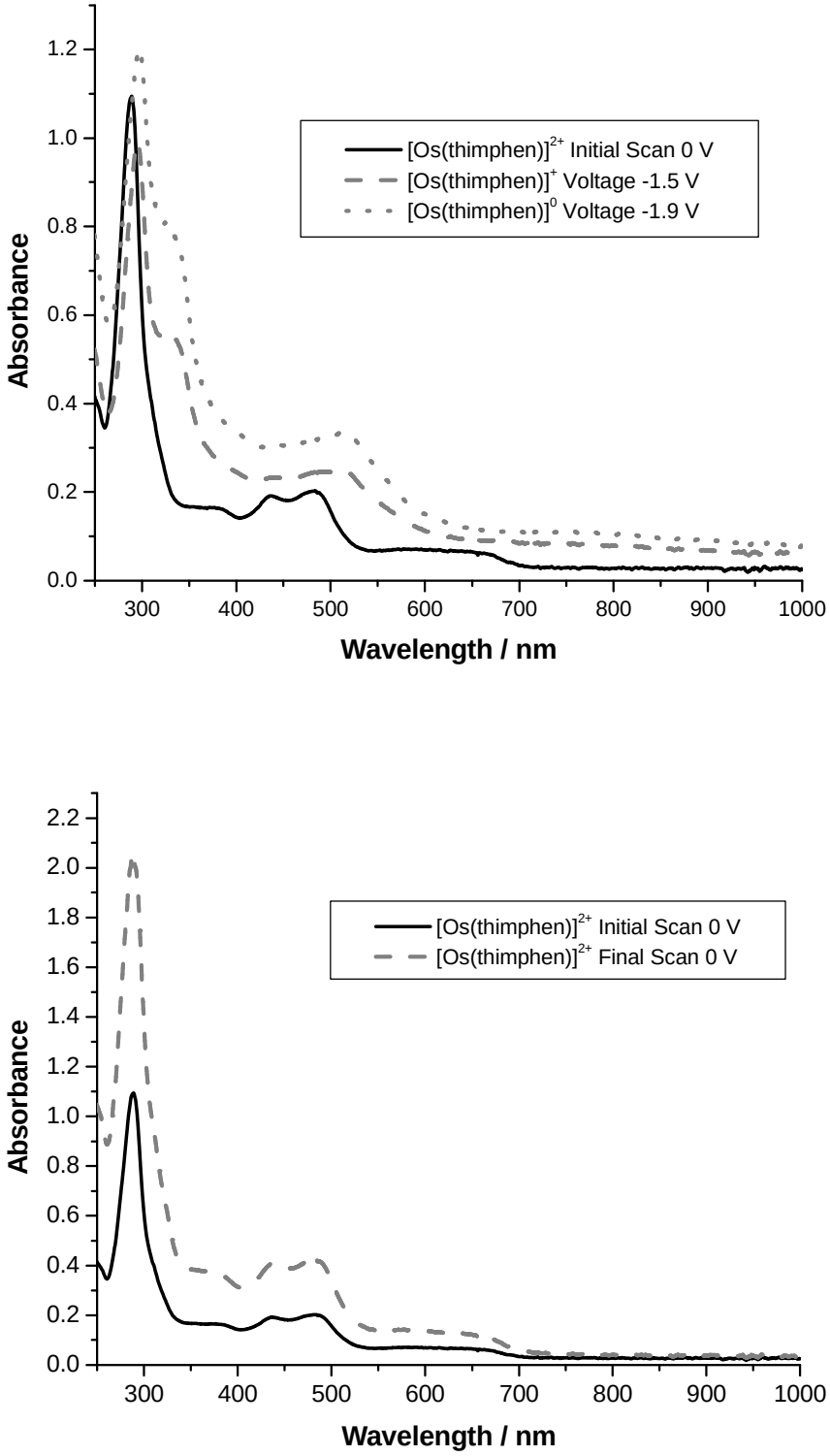

Figure 3.17: *Reductive spectroelectrochemistry of Os(thimphen) using a Pt gauze working electrode, vs. Ag wire, in 0.1 M TBAPF$_6$ in acetonitrile as the supporting electrolyte. The solution was degassed using Argon.*

Comparing the spectra of $[Os(pyrphen)]^{2+}$ with that of the monocationic complex, $[Os(pyrphen)]^{+}$ (bulk electrolysis at -1.3 V, *vs.* Ag wire) it is noted that the changes observed in the spectra of $[Os(pyrphen)]^{+}$ are less pronounced than those observed for the $[Os(thimphen)]^{+}$ complex, Figure 3.18 and Figure 3.19. The first reduction of Os(pyrphen) is a quasi-reversible process that is dependent on scan rate. The intensity of the absorbance bands, associated with the bipy anion radical transitions, increases with each change to more negative potentials. Bulk electrolysis at 0 V (*vs.* Ag wire), allows for the re-oxidation to the $[Os(pyrphen)]^{2+}$ complex. The corresponding spectrum obtained includes certain minor differences when compared to the original spectrum recorded prior to electrolysis. This is expected due to the quasi-reversible nature of this first cathodic process at slow scan rates. The irreversibility of the changes in the spectrum along with the considerable difference in intensity of the bipy anion radical bands between the two complexes may suggest, along with the electrochemical data, that the first reduction and hence the LUMO level is not associated with a bipy unit on the Os(pyrphen) complex. Instead the LUMO can be assigned as located on the pyrphen ligand itself.

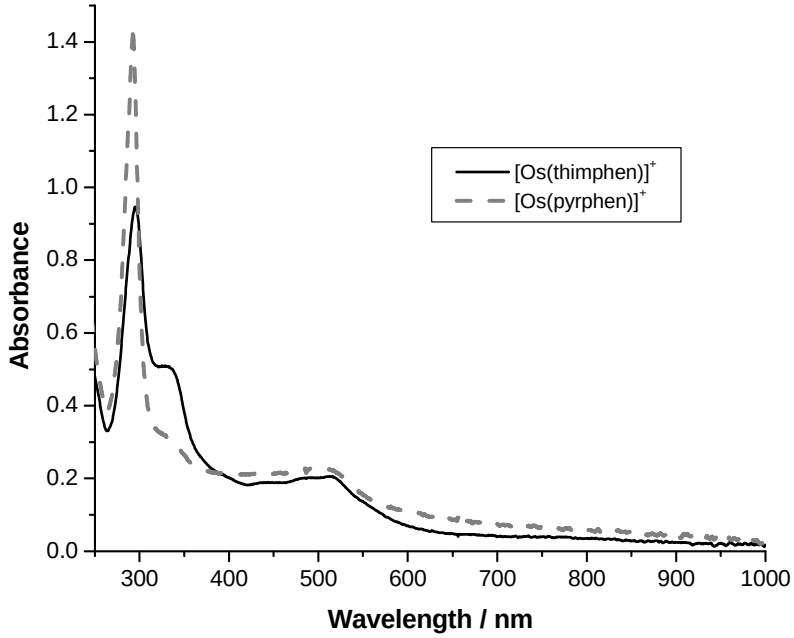

Figure 3.18: *Reductive spectroelectrochemistry of* $[Os(pyrphen)]^{+}$ *and* $[Os(thimphen)]^{+}$ *comparing the spectra of the first ligand reductions of each complex.*

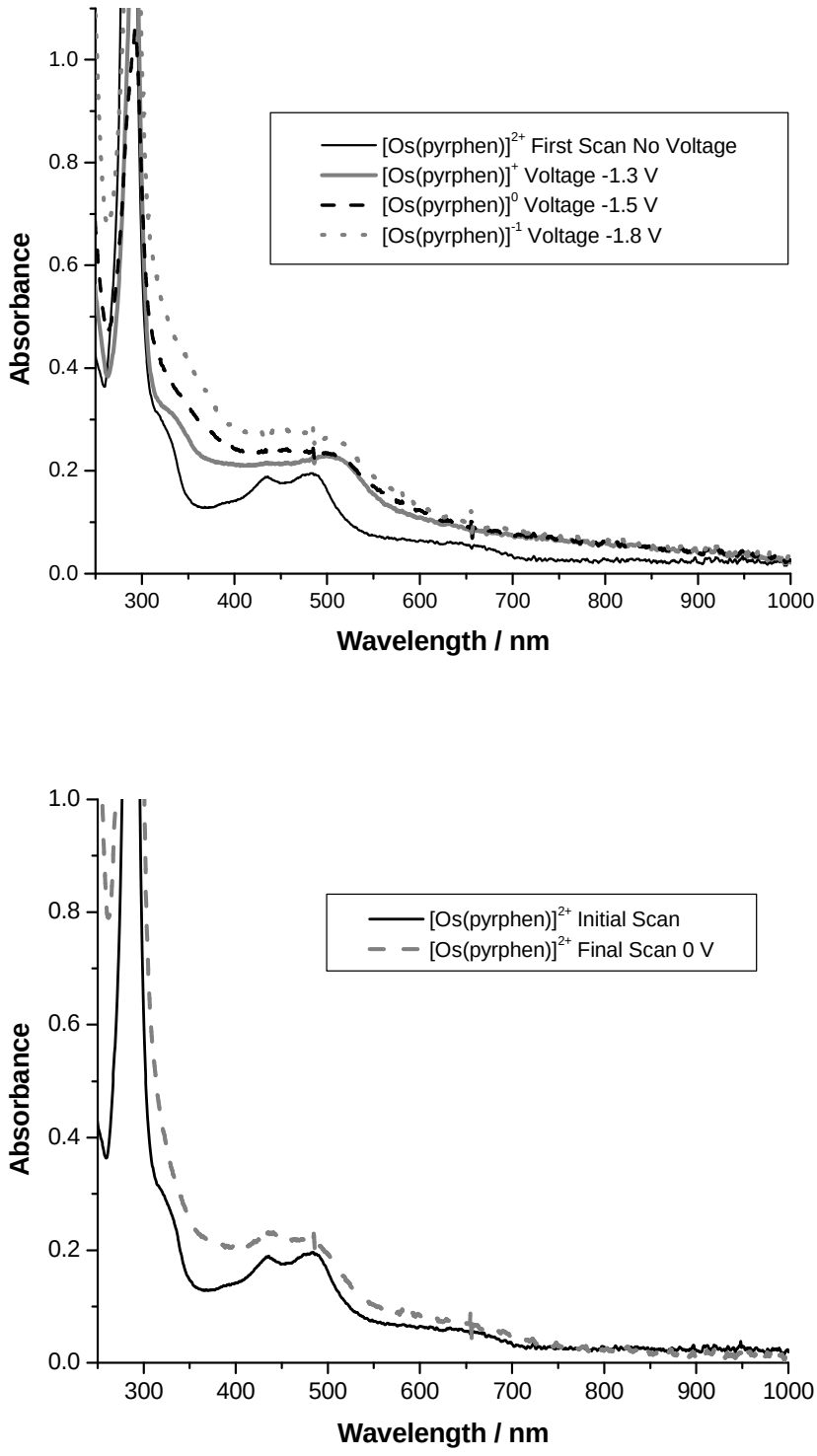

Figure 3.19: *Reductive spectroelectrochemistry of Os(pyrphen) using a Pt gauze working electrode, vs. Ag wire, in 0.1 M TBAPF$_6$ in acetonitrile as the supporting electrolyte. The solution was degassed using Argon.*

3.2.4 Raman Spectroscopy

The determination of certain properties of molecules such as the geometry of different molecular orbitals, the nature of electronic transitions and the energy levels of excited states is a relatively complicated process when using only a single spectroscopic technique. The use of several techniques, often in conjunction with one another is thus needed for a more comprehensive and reliable evaluation of the various results. In particular, specifying the location of the lowest excited state within a molecule is not possible by luminescence spectroscopy alone, the use of a technique like Raman spectroscopy provides invaluable information about the changes in vibrational energies upon excitation. Raman spectroscopy is a technique that investigates the inelastic scattering of light caused by the interaction of a photon with a molecule. Such an interaction leads to a change or increase in the state of each vibrational mode within. The intensity of the scattering is very low with only 1 in $10^8 - 10^{11}$ molecules within a sample producing the inelastic scattering of the photon.[29] Scattering effects can be greatly enhanced when Raman spectroscopy is conducted under resonant conditions as a result of the excitation wavelength coinciding with that of the electronic absorption band of the compound. Under these conditions an enhancement of the Raman scattering by factors as much as 10^6 can be achieved. Therefore, resonant Raman spectroscopy can provide useful information for assigning electronic transitions thanks to the enhancement of vibrational bands associated with that particular electronic transition.[30]

The vibrational modes of the excited states of Ru(pyrphen) and Ru(thimphen) were examined using excited state resonance Raman spectroscopy where each complex was irradiated with a short light pulse (9 ns) corresponding to a particular excitation wavelength of the complexes, Figure 3.20. The resulting Raman spectrum of each complex is compared with that of the excited state spectrum of $[Ru(bipy)_3]^{2+}$. Excitation at a wavelength that corresponds to an allowed transition such as Ru $\rightarrow \pi^*$ (bipy) will lead to enhancement of the symmetric stretching modes associated with the bipy ligand. Prominent peaks corresponding to the Raman scattering from the vibrational modes of the $bipy^{\bullet-}$ can be seen in the Raman spectrum as a result. The lowest lying excited state of $[Ru(bipy)_3]^{2+}$ is now widely accepted as a ^{3}MLCT transition involving a bipyridyl ligand.[20] Therefore the presence or absence of Raman

shifts, such as those of the $bipy^{\bullet-}$ of $[Ru(bipy)_3]^{*2+}$ (where * denotes an excited state) in the excited state, in the spectra of the ruthenium monomers will be used as an indicator of the location of the lowest lying excited state.

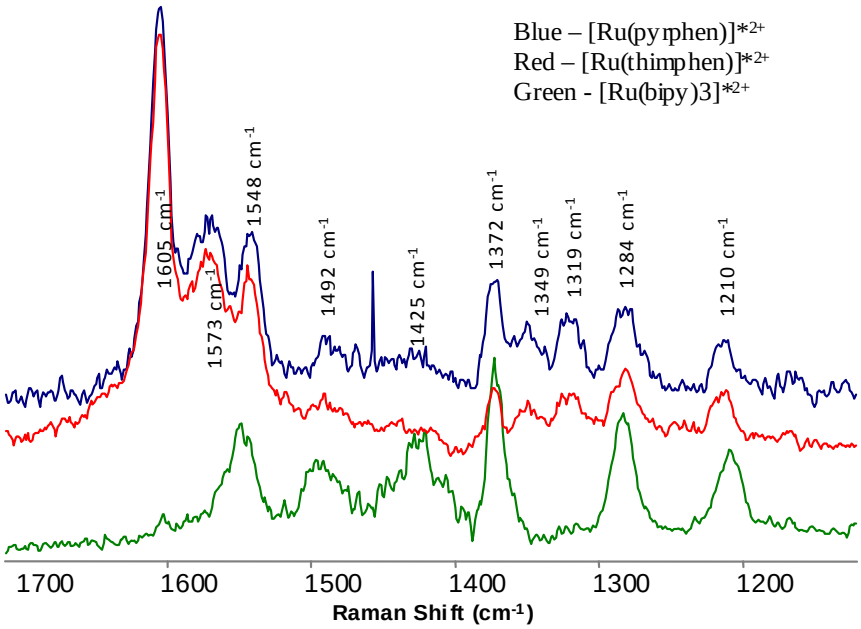

Figure 3.20: *Resonance Raman spectra of* $[Ru(pyrphen)]^{*2+}$ *(blue line),* $[Ru(thimphen)]^{*2+}$ *(red line) and* $[Ru(bipy)_3]^{*2+}$ *(green line) in acetonitrile. The excitation wavelength used was 355 nm.*

The excited state resonance Raman spectroscopy of these complexes was carried out by Dr. Wesley R. Browne in the University of Groningen, The Netherlands. The spectrum of each complex is shown in Figure 3.20. Excitation with a 9 ns pulse at 355 nm on the complexes allowed for promotion to an electronically excited state of the complexes under investigation. The choice of this wavelength allows the determination of the possible involvement of the π* orbital of a bipy unit in MLCT transitions since at this wavelength the bipy anion radical presents an absorption peak. In fact, the resulting MLCT transition involves a change in the electronic charge distribution through a transfer of electron density from the ruthenium metal centre of $[Ru(bipy)_2(L)]^{2+}$, where L = pyrphen/thimphen, to either a bipy ligand or the pyrphen/thimphen ligand. The nature of the ligand that receives charge from the metal centre depends on the location of its lowest lying π* orbital.

Each excited state complex exhibits Raman shifts characteristic of these vibrational modes of the $bipy^{\bullet-}$. These are observed at 1548, 1495, 1427, 1365, 1285, 1212 and 1164 cm^{-1} as has been observed for a similar ruthenium mononuclear complex, $[Ru(bipy)_3]^{*2+}$.[31] The neutral bipy ligand exhibits Raman shifts at 1608, 1563, 1491, 1450, 1320, 1276 and 1176 cm^{-1}.[32] The shifts in the spectra corresponding to those of the anion radical of the bipy ligand are clearly visible in both Ru(pyrphen) and Ru(thimphen). This would suggest, contrary to results obtained from electrochemistry and spectroelectrochemistry where the excited species are proposed to be $[Ru^{II}(bipy)(bipy^{\bullet-})(thimphen)]$ and $[Ru^{II}(bipy)_2(pyrphen^{\bullet-})]$ (*vide supra*), that the lowest lying excited state of each complex involving a ^{3}MLCT transition is localised on a bipyridyl ligand and not on the pyrphen or thimphen ligands where the excited state of the complex is represented by $[Ru^{III}(bipy)(bipy^{\bullet-})(L)]$. The remaining bands are therefore assigned to the Raman scattering from the vibrational modes associated with the neutral phenanthroline type ligand (1349 and 1573 cm^{-1}) as they do not appear in the spectrum of $[Ru(bipy)_3]^{2+}$, Figure 3.20. These bands are also observed in the SERS spectra of each of the complexes; *vide infra* (Section 3.2.5.2).

3.2.5 Electrochemical and Raman Spectroscopical Properties of Mononuclear Complexes Confined on a Surface

3.2.5.1 Electrochemical Properties of Surface Confined Complexes

The formation of monolayers of chemical species, whether they are self-assembled or spontaneously adsorbed, involves the binding of a surface active functional group within the molecule to a surface. Both types of monolayers differ in the degree of lateral interaction between the adsorbates on the surface. Self-assembled monolayers work to stabilize lateral interactions between the redox active species on the surface. The substrate choice can be of particular importance when forming monolayers. Long range ordered monolayers offer more facile control and manipulation of the properties of the monolayer. Substrate metals, e.g. Au, Ag or Pt, differ in their surface properties and as a result can affect the physical and chemical properties of the monolayer. The structure and defect density of a monolayer will change depending on the properties of the substrate. Electrochemical and photophysical properties of the species within the monolayer can also be altered depending on the associated substrate.[33] Molecular electronics is concerned with assembling molecules on an electrode surface, in a

manner in which they will be able to conduct and switch electrical currents, and using these systems to replace components in solid state electronic devices such as transistors, wires and diodes. With this concept in mind, monolayers of all four mononuclear complexes discussed in this chapter have been formed using Pt and Au metals as the substrate for binding.

The process of self-assembly of a species on a substrate is a relatively simple process in which the monolayer will form under atmospheric pressure and at room temperature. In the context of the complexes discussed in this chapter it was not necessary to prepare anhydrous or anaerobic solutions for the deposition procedure. Simply exposing the substrate to solutions of each complex over time (overnight for each complex in this chapter) is sufficient for assembly. The solvent used for the immersion process is chosen based on the solubility of the species and does not affect the assembly process Concentrations in the range of micro to millimolar are generally used – bearing in mind that the concentration may affect the homogeneity of the resulting layer.[34]

Monolayers of Ru(pyrphen) and Ru(thimphen) were formed on a Pt macro electrode following overnight immersion in 500 μM solutions of Ru(pyrphen) in dimethylformamide(DMF)/H_2O (1:1) and Ru(thimphen) in ethanol. The Faradaic response obtained for both complexes is a direct result of the species on the electrode surface as neither complex was added to the electrolyte solution prior to the experiment. Also, any unbound residue of the complex that was not removed with rinsing of the electrode will give rise to a concentration so low that it would not affect the Faradaic response.

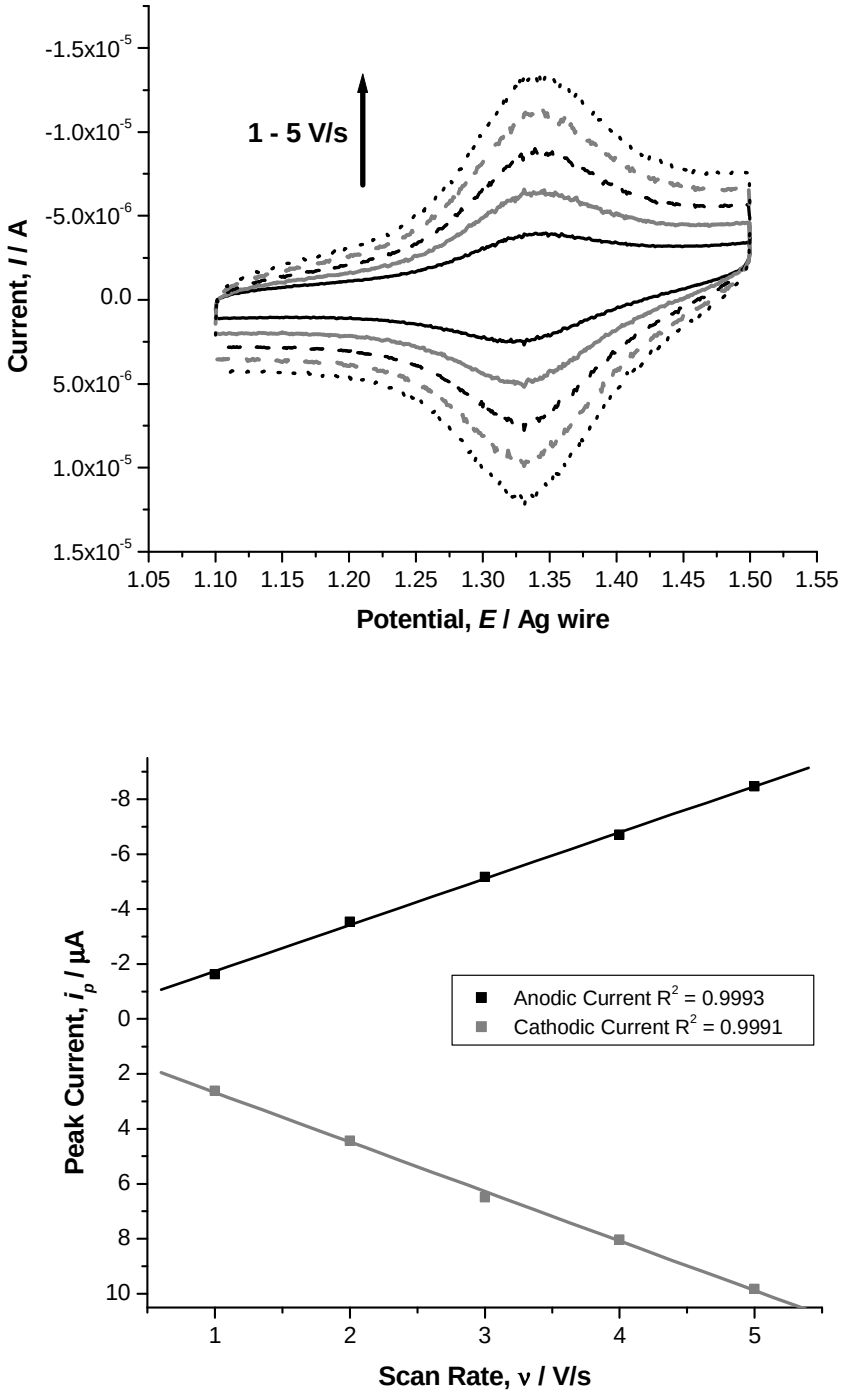

Figure 3.21: *Cyclic voltammetry of a monolayer of Ru(pyrphen) (top) on a Pt macro electrode (real surface area = 0.1041 cm^2) following immersion overnight in a 500 µM solution of the complex in DMF/H_2O (1:1), vs. Ag wire, using 0.1 M TBAClO_4 in acetonitrile as the supporting electrolyte. Bottom: graph illustrating the linear relationship between the peak current, i_p, versus the scan rate, v.*

Both complexes form stable monolayers on Pt macro electrodes, the cyclic voltammograms of which are shown in Figure 3.21 and Figure 3.22. The scan rate of the cyclic voltammograms was varied from 1 – 5 V/s and the peak shape and potential do not change with changes in scan rate. The observed current i_p (A) is directly proportional to the scan rate, ν (V/s) which is consistent with a surface confined species rather than a diffusion controlled process where i_p is proportional to $\nu^{½}$. Monolayers exhibiting ideal reversible redox responses have an anodic to cathodic peak separation, ΔE_p equal to 0 V. ΔE_p values of less than 15 mV and 25 mV have been calculated for Ru(pyrphen) and Ru(thimphen) respectively. These non-zero values can indicate the presence of intermolecular interactions between the molecules on the surface when oxidised. Alternatively, this can also suggest a degree of reorganization within the monolayer following the applied potential. The full width at half maximum, FWHM is 90.6 mV calculated for a one electron reversible reaction showing Nernstian behaviour.[33] The monolayers of both ruthenium complexes have FWHM values greater than this theoretical value of 90.6 mV ranging from 100 – 110 mV for Ru(pyrphen) and 115 – 150 mV for Ru(thimphen). The FWHM was calculated from the Faradaic current response thereby excluding any contribution from the capacitive current.

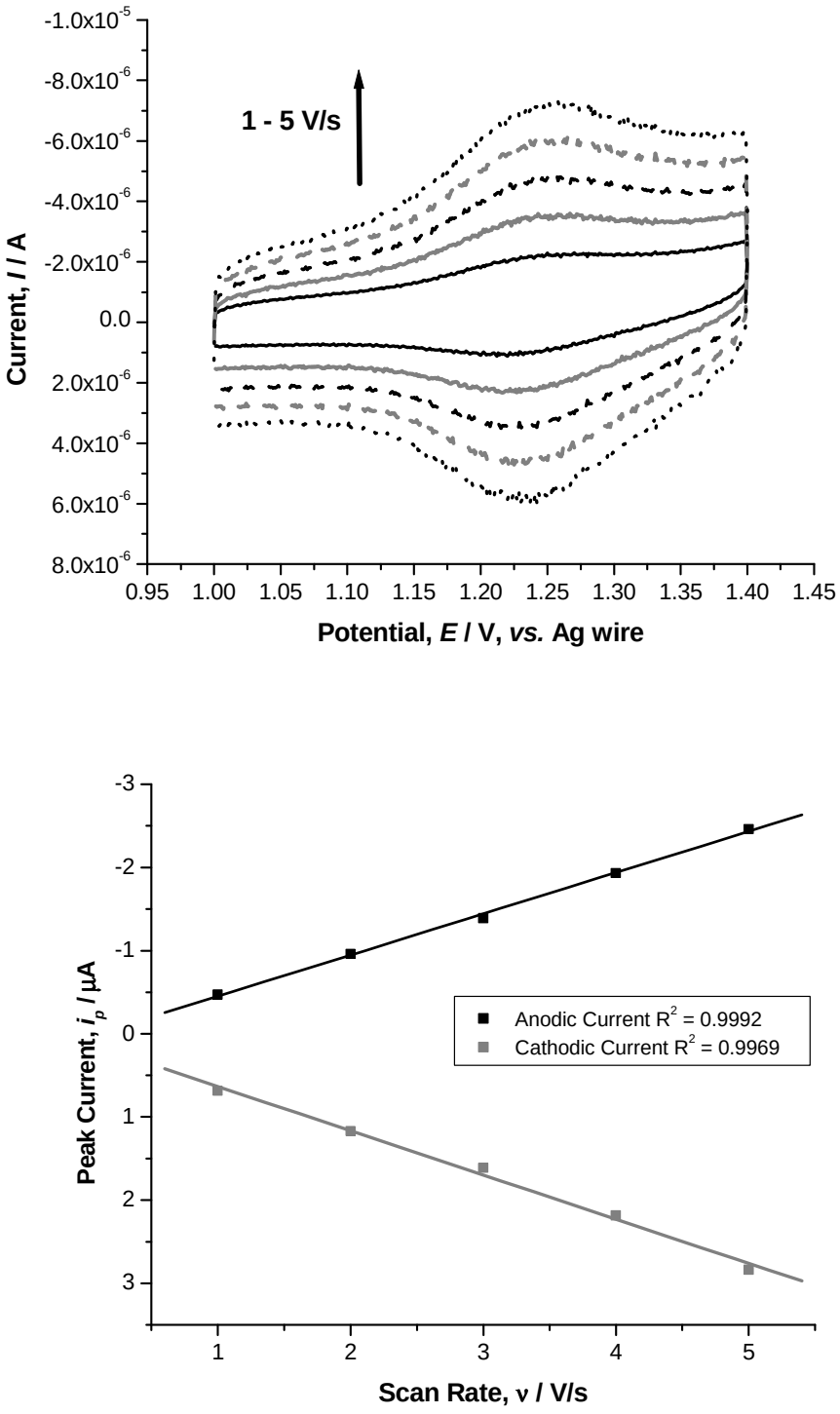

Figure 3.22: *Cyclic voltammetry of a monolayer of Ru(thimphen) (top) on a Pt macro electrode (real surface area = 0.0982 cm^2) following immersion overnight in a 500 µM solution of the complex in ethanol, vs. Ag wire, using 0.1 M TBAClO$_4$ in acetonitrile as the supporting electrolyte. Bottom: graph illustrating the linear relationship between the peak current, i_p, versus the scan rate, v.*

This may suggest that lateral interactions exist between the molecules mounted on the surface and that they are repulsive toward each other. Attractive interactions give rise to FWHM values of less than 90.6/n mV, where n = the number of electrons transferred.[33] It is also possible that these values arise as a result of a distribution of formal potential within the monolayer caused by a disorganised orientation of the molecules or differing electrostatic environments around the redox centres within. Although evidence of lateral interaction exists between the molecules on the surface, the behaviour of the molecules within the monolayer can be described as close to ideal. This has also been observed for a similar ruthenium polypyridyl complex, $[Ru(bipy)_2(bipySH)]^{2+}$, where thiol groups (SH) act as the surface linker to Pt electrodes.[35] A ΔE_p value of 15 ± 5 mV and FWHM of 110 ± 10 mV were reported for this monolayer with a surface coverage of 8.1 x 10^{-11} mol cm^{-2}. Monolayers of another ruthenium mononuclear complex reported by Forster *et al.* [36] have a surface coverage in the range of 0.2 – 1.0 x 10^{-10} mol cm^{-2}. The FWHM of the voltammetric peaks of this monolayer increases with increasing surface coverage indicating increasing destabilising lateral interactions as the distance between adsorbates decreases. As the peak potentials, E_p of the Ru complexes discussed in this chapter do not change with increasing scan rates ohmic effects and an increasing iR drop are not considered influential toward the observed electrochemical response of the monolayers.[14a]

The surface coverage of each of the monolayers has been calculated, Table 3.5. As the concentration of the redox active species in the electrolyte solution is zero, or approximately zero, the observed Faradaic response is assumed to originate from the monolayer adsorbed on the surface of the electrode. Therefore the total Faradaic charge injected into the monolayer upon oxidation of the redox active species can be obtained from the area under the corresponding wave in the cyclic voltammogram (excluding the contribution from the capacitive current) and can be related to the surface coverage through Equation 3.3.

Equation 3.3 $\Gamma = Q/nFA$

where Γ represents the surface coverage in mol cm^{-2}, Q is the Faradaic charge, n is the number of electrons involved in the redox process, F is the Faraday constant and A is

the real surface area of the electrode.[33] Using the values obtained for the surface coverage, the average area that each molecule occupies, A_{molec} (Å^2) can be calculated from Equation 3.4.

Equation 3.4 $$A_{molec} = 10^{16} / N_A \Gamma$$

where N_A is the Avogadro constant. The surface coverage calculated for each complex corresponds to a molecular area of occupation of 885 and 2560 Å^2 for each molecule within the monolayer of Ru(pyrphen) and Ru(thimphen) respectively. This area per molecule is a lot larger than would be expected for closely packed monolayers of these complexes considering the projected area for these types of ruthenium polypyridyl complexes is approximately 90 Å^2. The values obtained for FWHM of the voltammetric peaks of these monolayers are greater than the theoretical value of 90.6 mV for a one-electron process.[17] Considering this result and the molecular area of occupation on the surface it seems likely that repulsive interactions exist between adjacent molecules on the surface, a factor which was also observed for the similar ruthenium complex reported by Forster *et al.*[35] The orientation of the molecule within the monolayer and the possibility that these complexes do not form well ordered, closely packed monolayers must also be considered.

Monolayer	**$E_{½}$, vs. SCE Solution Phase**	**$E_{½}$, vs. SCE Monolayer**	**Surface Coverage, Γ (mol / cm^2)**
Ru(pyrphen)	+1.31 V	+1.33 V	$1.9 \pm 0.02 \times 10^{-11}$
Ru(thimphen)	+1.30 V	+1.24 V	$6.5 \pm 0.2 \times 10^{-12}$

Table 3.5: *Half-wave potentials of the solution phase and surface confined complexes and calculated surface coverage for the monolayers of Ru(pyrphen) and Ru(thimphen) at a Pt substrate.*

The four mononuclear ruthenium and osmium complexes have been synthesised and characterised for potential applications such as the development of molecular transistors. For molecules to be considered potentially useful as molecular transistor they are required to have a stable redox centre that exhibits reversible electrochemical properties. The formation of stable well behaved monolayers on an electrode surface

is also required. Characterising the orientation and tunnelling currents of these complexes within a monolayer can be carried out using an in-situ electrochemical scanning tunnelling microscopy (STM) setup at room temperature.[13] The redox potential of Ru(pyrphen) and Ru(thimphen) is higher than that of water and as potential STM experiments are carried out in aqueous solutions, and therefore at potentials less positive than 1.0 V (*vs.* SCE), monolayers of the osmium analogues on Au and Pt are deemed more suitable for this particular application.

Monolayer	$E_{½}$ **/ V Solution Phase ACN**	$E_{½}$ **/ V Monolayer ACN**	$E_{½}$ **/ V Monolayer H_20**	**Surface Coverage, Γ (mol / cm^2)**
Os(pyrphen)	+0.86 (Pt)	+0.88 (Pt)	+0.67 (Pt)	$1.1 \pm 0.02 \times 10^{-11}$ (H_2O)
				$2.1 \pm 0.02 \times 10^{-11}$ (ACN)
Os(thimphen)	+0.83 (Pt)	+0.93 (Au)	+0.68 (Au)	$3.2 \pm 0.02 \times 10^{-11}$ (H_2O)
				$1.8 \pm 0.02 \times 10^{-11}$ (ACN)

Table 3.6: *Half-wave potentials, vs. SCE, of the solution phase and surface confined complexes, in H_2O and acetonitrile along with the calculated surface coverage for the monolayers of Os(pyrphen) and Os(thimphen) on Pt and Au substrates. The working electrode is specified in parentheses.*

Stable monolayers of each of the osmium complexes have been formed on both platinum and gold electrodes. The electrochemical response from the monolayers was investigated using both acetonitrile and water as the electrochemical solvent. $LiClO_4$ was used as the electrolyte for the aqueous system. As this compound is insoluble in acetonitrile a second perchlorate electrolyte, $TBAClO_4$ was used instead. The cyclic voltammetry of the monolayers formed are shown in Figure 3.23 to Figure 3.28 along with the graphs illustrating the relationship between the peak current and the scan rate. A linear relationship between the peak current and the scan rate has been obtained for both complexes indicating that a monolayer has been formed on the surface and the Faradaic current response is not associated with a diffusive process.

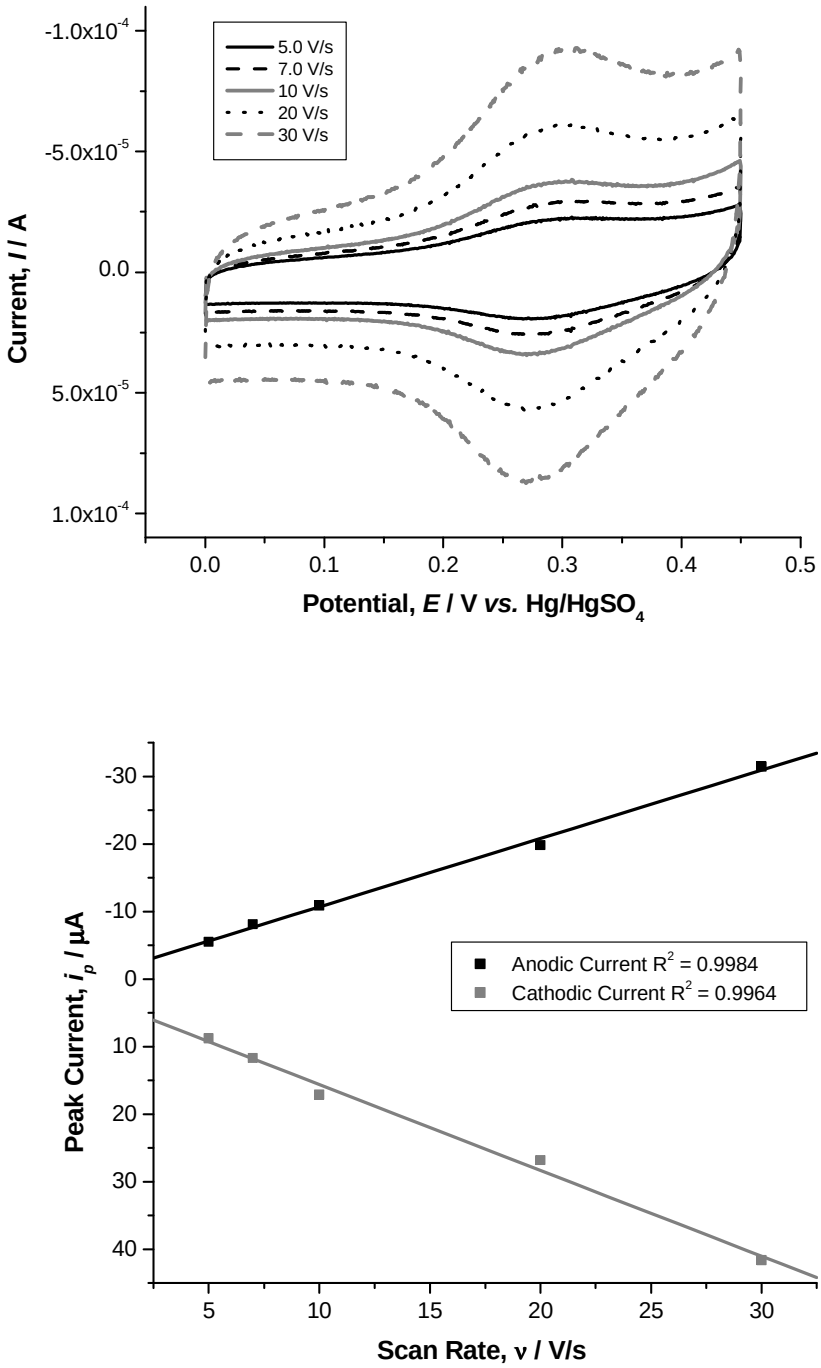

Figure 3.23: *Cyclic voltammetry of a monolayer of Os(pyrphen) (top) on a Pt macro electrode (real surface area = 0.1223 cm^2) following immersion overnight in a 500 µM solution of the complex in DMF/H_2O (1:1), vs. Hg/$HgSO_4$, using 0.1 M $LiClO_4$ in H_2O as the supporting electrolyte. Bottom: graph illustrating the linear relationship between the peak current, i_p, versus the scan rate, v.*

Monolayers of Os(pyrphen), in aqueous electrolyte (Figure 3.23), on a Pt substrate reveal a greater degree of lateral interaction between the adsorbates on the surface compared to the same system in acetonitrile. This is observed through such properties as the FWHM (105 – 135 mV), the separation between the peaks ΔE_p (30 mV) and the surface coverage, Table 3.6. In acetonitrile the FWHM of this complex ranges from 110 – 115 mV and the distance between the anodic and cathodic voltammetric peaks is 20 mV. The monolayer in acetonitrile has a surface coverage of the same order of magnitude as that of the aqueous system, 10^{-11} mol cm^{-2}. Using the values for the surface coverage, the projected area of occupation per molecule of the Os(pyrphen) in each monolayer was calculated. It was found that one molecule occupies an area of 780 $Å^2$ on the substrate, recorded in acetonitrile electrolyte. This value was doubled when calculated from voltammetric peaks recorded in an aqueous environment (1480 $Å^2$). Similar osmium polypyridyl complexes have been reported where the crystallographic data reports radii of 7.5 Å for these types of compounds.[37] Based on this, the proposed area per molecule for a similar osmium complex, $[Os(bipy)_2(p0p)Cl]^+$ where p0p is 4,4-bipyridyl, is 180 $Å^2$.[14a] This information would suggest that the packing density within the monolayer involves adsorbates that are separated by significant distances. This can also suggest that, like the monolayers of the Ru complexes, the orientation of the molecules on the surface may be more complicated than the ideal situation where the molecules stand perpendicular to the surface of the electrode. The differing responses obtained from the monolayers in each solvent are not hugely significant however these results suggest that repulsive interactions exist within the monolayer (FWHM > 90.6/n mV [33]) in both acetonitrile and water. The electrochemistry of the monolayers of Ru(pyrphen) and Ru(thimphen) was not examined in aqueous electrolyte as the oxidation potential of the ruthenium metal centre is more positive than that of water. As such, the projected area per molecule of each ruthenium complex in aqueous electrolyte was not investigated.

The difference between the anodic and cathodic peak potentials, recorded for the monolayer of Os(thimphen), Figure 3.24, is constant in an aqueous electrolyte with a ΔE_p of 65 mV whereas this value increases with increasing scan rate in acetonitrile. Similar behaviour is observed when considering the FWHM in both the aqueous and organic environments. In an aqueous electrolyte the FWHM ranges from 110 – 130 mV whereas a range of 140 – 160 mV is recorded in acetonitrile. These values

obtained for both the ΔE_p and FWHM are greater than the corresponding values associated with a monolayer exhibiting ideal electrochemical responses (ΔE_p of 0V and FWHM of 90.6/n mV).

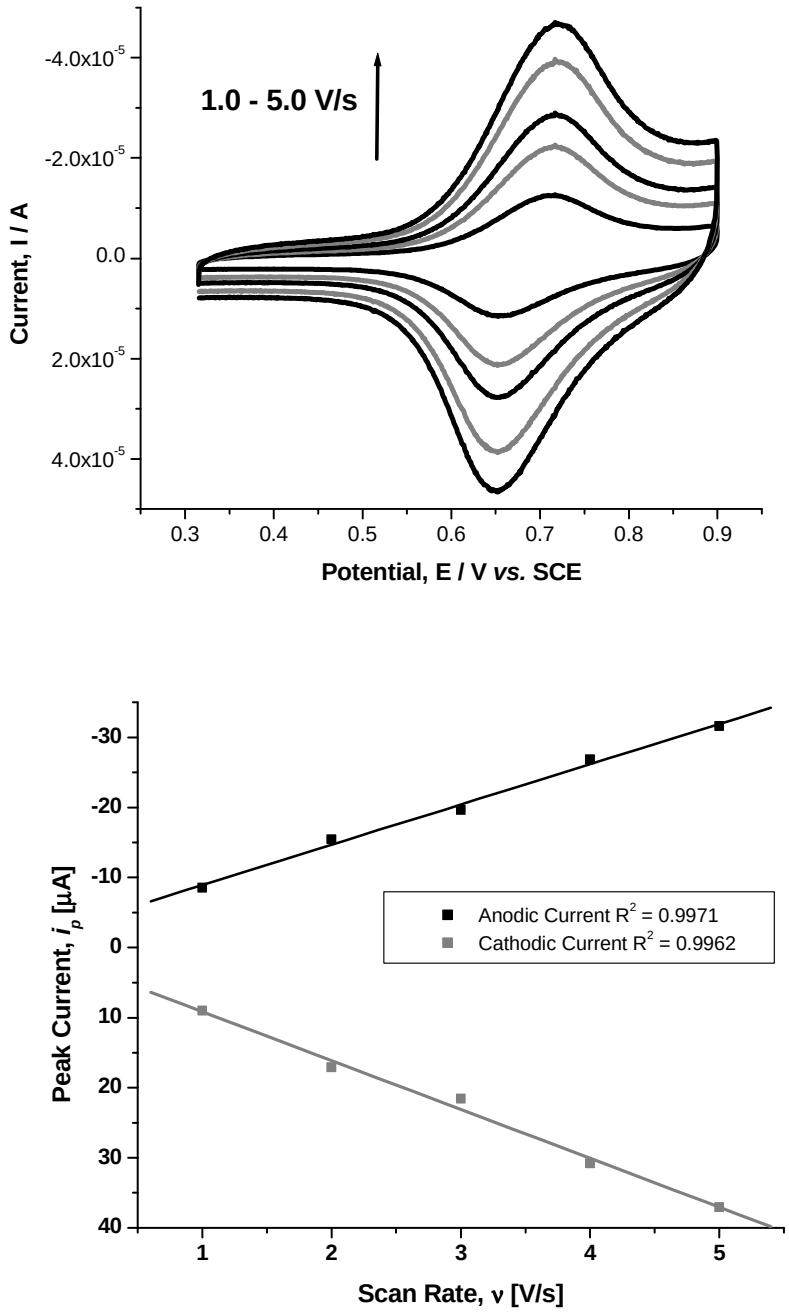

Figure 3.24: *Cyclic voltammetry of a monolayer of Os(thimphen) on a Au bead electrode (real surface area = 0.0424 cm^2) following immersion overnight in a 500 μM solution of the complex in ethanol, vs. SCE, using 0.1 M $LiClO_4$ in H_2O as the supporting electrolyte. Bottom: graph illustrating the linear relationship between the peak current, i_p, versus the scan rate, v.*

A surface coverage of 3.2 x 10^{-11} mol cm^{-2} has been calculated for Os(thimphen) in aqueous electrolyte which leads to a projected area per molecule of 530 $Å^2$. This is double that of the projected area per molecule reported for a monolayer of a similar osmium complex, $[Os(bipy)_2(p0p)Cl]^+$ [14a] (240 $Å^2$) suggesting that the Os(thimphen) molecules are less ordered on the surface of the substrate. Another possible explanation may be the existence of greater lateral interaction in the latter which would result in a greater distance between the molecules, as reflected by the large FWHM values obtained. The calculated surface coverage of the Os(thimphen) monolayer on Au in acetonitrile decreases by approximately a half from 1.8 x 10^{-11} to 5.6 x 10^{-12} mol cm^{-2} following the initial scanning at 10 V/s per second for 8 sweep segments, Figure 3.25. The diffusion controlled electrochemistry was carried out using acetonitrile as the electrochemical solvent as all four complexes are fully soluble in this solvent. This increased solubility in acetonitrile compared to aqueous electrolytes may be the cause of the decrease in the surface coverage of Os(thimphen) in acetonitrile compared to that calculated for the monolayer of the complex in water.

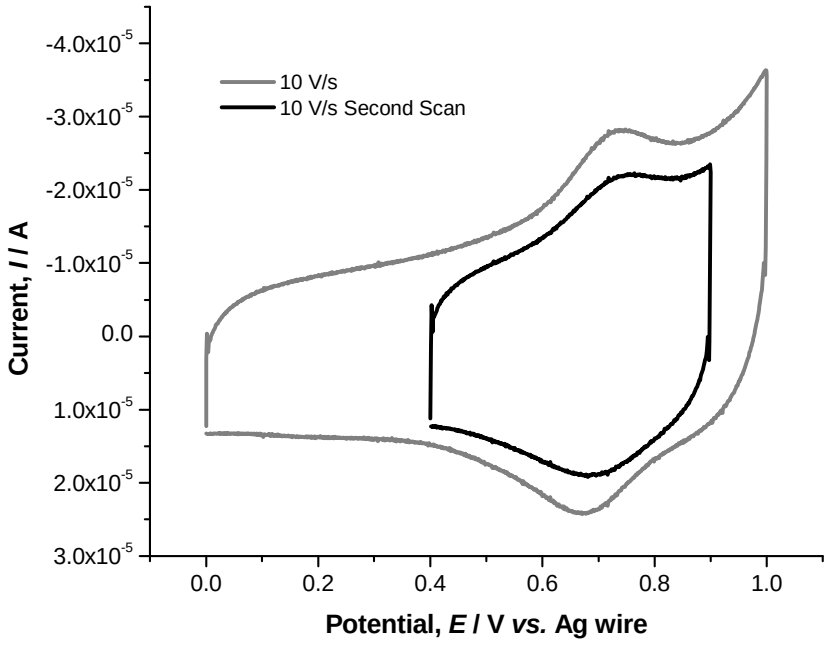

Figure 3.25: *Cyclic voltammetry of a monolayer of Os(thimphen) on a Au bead electrode (real surface area = 0.0514 cm^2), vs. Ag wire, using 0.1 M $TBAClO_4$ in acetonitrile as the supporting electrolyte. A substantial decrease in the intensity of the peak current is observed in the second of two consecutive scans at 10 V/s.*

In the cyclic voltammograms of both the Os(pyrphen) and Os(thimphen) monolayers recorded in aqueous electrolyte, Figure 3.23 and Figure 3.24 respectively, the resulting capacitive current, following oxidation of the metal centre to Os^{3+}, is greater than that of the background current produced prior to oxidation as well as that observed following reduction back to the Os^{2+} state. The oxidation potential of these metal complexes is close to that of the oxidation potential of water.

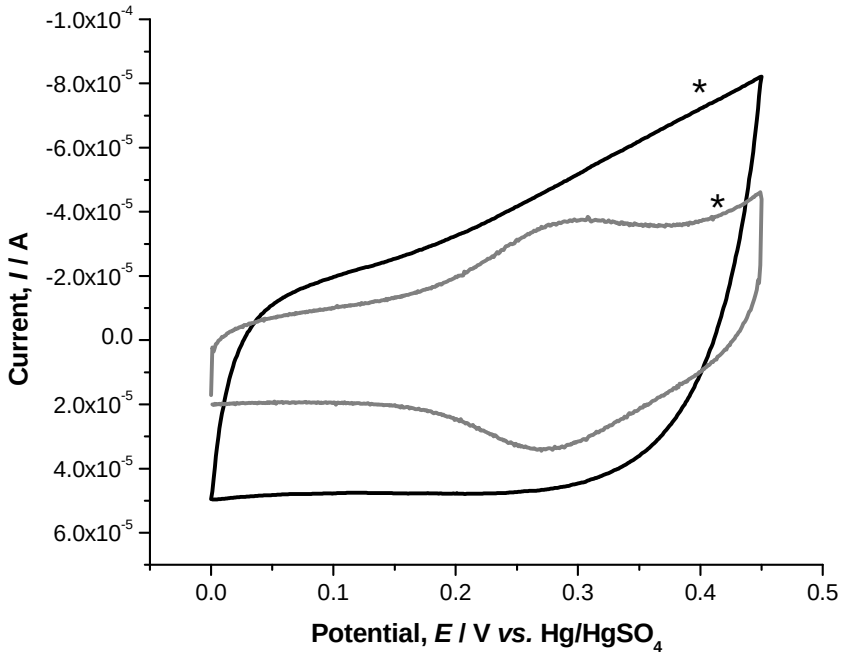

Figure 3.26: *Cyclic voltammetry of the Os(pyrphen) monolayer (grey) with the solvent blank (black) on a Pt macro electrode, vs. $Hg/HgSO_4$, at 10 V/s using 0.1 M $LiClO_4$ in H_2O as the supporting electrolyte.*

In aqueous electrolyte the potential window used was between +0.3 and +0.9 V, *vs.* SCE. It is possible that the resulting increase in the current is not a result of an increase in capacitive current but instead is due to the oxidation of the aqueous electrolyte. Figure 3.26 shows a CV of the Os(pyrphen) monolayer recorded at 10 V/s overlaid with the aqueous electrolyte blank recorded at the same scan rate. This increase in the current (marked with * in Figure 3.26) is also observed in the solvent blank indicating that it is associated with the aqueous electrolyte and is not a

consequence of increased capacitive current following oxidation of the metal centre. This effect is also less pronounced in organic electrolyte, Figure 3.27.

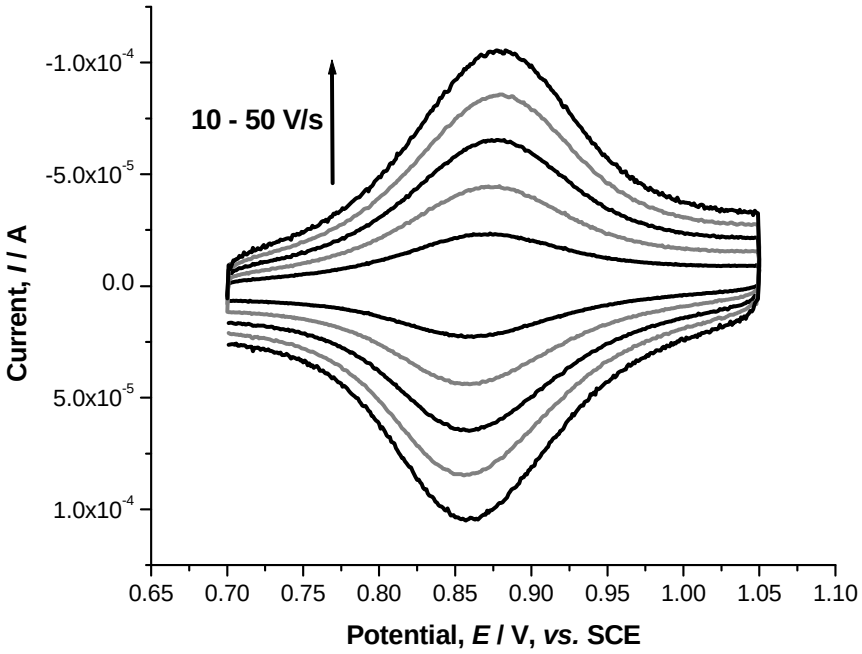

Figure 3.27: *Cyclic voltammetry of a monolayer of Os(pyrphen) on a Pt macro electrode (real surface area = 0.1154 cm^2) following immersion overnight in a 500 μM solution of the complex in DMF/H_2O (1:1), vs. SCE, using 0.1 M $TBAClO_4$ in acetonitrile as the supporting electrolyte.*

For the electrochemical characterisation of the monolayers a cyclic voltammogram was obtained for each different scan rate by cycling between the initial and final potential for 8 sweep segments. The CVs obtained for the monolayers of Os(thimphen) contain a feature that is not observed in the cyclic voltammetry of the monolayers of any of the previous three complexes discussed. The first sweep segment of each scan reveals an anodic peak potential that is approximately 40 mV more positive than the anodic peak potentials of each consecutive sweep segment obtained thereafter, Figure 3.28. This trend continues with each change in scan rate. It is also noted that this is only observed for the monolayers of Os(thimphen) and not the analogous ruthenium complex or either of the M(pyrphen) complexes. It must also be

pointed out that this potential shift behaviour does not occur in organic solvent but is observed in aqueous electrolyte only although the anionic component in both systems is a perchlorate ion.

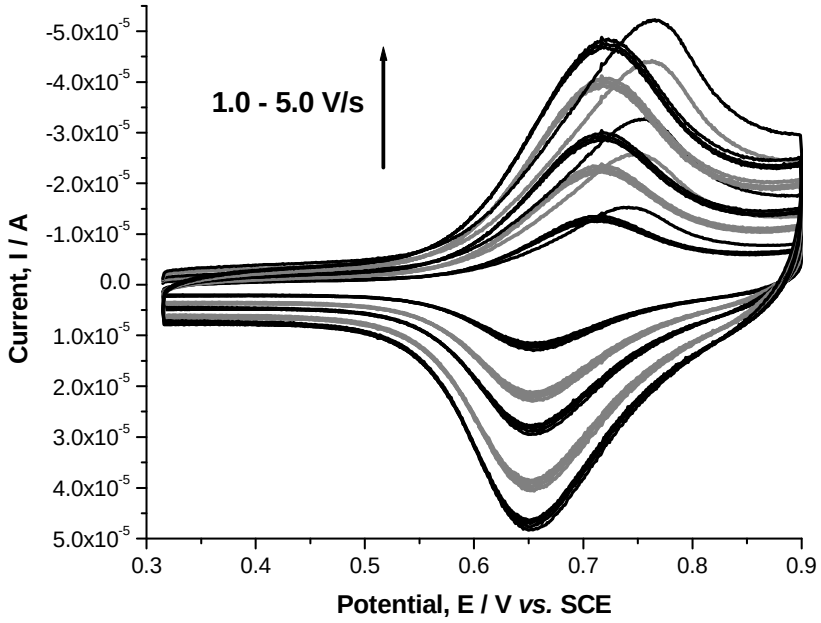

Figure 3.28: *Cyclic voltammetry of a monolayer of Os(thimphen) on a Au bead electrode (real surface area = 0.0424 cm^2) following immersion overnight in a 500 μM solution of the complex in ethanol, vs. SCE, using 0.1 M $LiClO_4$ in H_2O as the supporting electrolyte. Each CV is made up of 8 sweep segments.*

Forster and Faulkner [14a] investigated the effects of ion pairing on a similar osmium complex, $[Os(bipy)_2(p0p)Cl]^+$. By changing the concentration of the perchlorate electrolyte, and monitoring the effect on the formal potential, the extent of ion pairing around the redox centres within the monolayers was examined. This was investigated using both aqueous and organic electrolyte solvents. It was observed that the formal potential, E^o, experienced shifts toward more negative potentials with each increase in electrolyte concentration indicating that the redox centre is more easily oxidised in high electrolyte concentrations and experiences ion pairing from the anions in the electrolyte. A plot of E^o versus the log of electrolyte concentration is linear with a theoretical slope of 59/*p* mV / decade where *p* is the number of perchlorate electrolyte anions paired with the oxidised redox centre. In an organic tetrahydrofuran electrolyte

it was found that a single perchlorate ion is paired with the redox centre in the reduced Os^{+} state. Upon oxidation to Os^{2+} a second perchlorate anion becomes strongly bound to the monolayer as the slope obtained was 51 mV / decade, indicating that only one anion is added to the oxidised complex. However, in aqueous electrolyte two perchlorate ions become strongly bound to the redox centres within the molecule following oxidation (slope of 24 mV / decade) - thus suggesting that the reduced form is not ion paired.

It is possible that the observed shift in potential of the Os(thimphen) monolayer in aqueous solution, following initial oxidation to the Os^{3+} state, arises as a result of the uptake of perchlorate ions that then become trapped within the monolayer: this can lead to a certain degree of stabilisation within the monolayer thereby lowering the oxidation potential of the metal centre as it is thermodynamically more facile in an ion paired state. Upon reduction, and in the experimental time taking to manually change the scan rate, the added anion may be released out of the monolayer allowing for the same structural rearrangement to occur with the next scan rate. Forster and Faulkner identified that the extent of ion pairing with these types of osmium complexes is strongly solvent dependent which may explain why this phenomena is observed in aqueous electrolytes only.[14a]

Table 3.6 includes the half-wave potentials of both of the osmium mononuclear complexes considering the diffusion controlled effects in solution as well as the surface confined processes in the monolayer system. It is noted that the oxidation potential of each osmium metal centre within the monolayer, in aqueous perchlorate electrolyte is approximately 200 – 250 mV less positive than that of the monolayer confined process in acetonitrile ($TBAClO_4$). The observed potential of Os(pyrphen) assembled on platinum in acetonitrile is, however, very similar to that of the diffusion controlled process even though the anion components of the electrolyte systems are different. Os(thimphen) within a monolayer on Au in acetonitrile is oxidised at a potential approximately 100 mV more positive than that of the complex in solution.

The effect of the solvent pH on the oxidation potential of the metal centres was considered as one possible reason for the difference in oxidation potential between the metal centres within the monolayer in aqueous electrolyte and in acetonitrile. In

aqueous electrolyte, the changes in the oxidation potential of the metal centre of each complex was monitored at each different pH using 0.1 M $HClO_4$ and 0.1 M LiOH as the acid and base respectively. Decreasing the pH from 8.5 to 1.1, brought about only small changes in the oxidation potential of Os(thimphen). Over this range, in order of reducing pH, the anodic peak potential was shifted toward more positive potentials by approximately 50 mV whereas the cathodic peak potential was only shifted by approximately 10 mV. Similar behaviour was observed for the monolayer of Os(pyrphen) on a Pt surface over a pH range of 8.4 to 1.7 with positive shifts of only 25 and 15 mV for the anodic and cathodic peak potentials respectively. Under basic conditions the monolayer is stable up to a pH of 9 with minimal changes observed in the oxidation potential of each complex. Increasing the pH above 9, results in stripping of the electrode surface and consequent loss of the voltammetric signal.

Given that the observed changes in potential under different acidic and basic conditions are small, it is proposed that a variation of pH is not the main cause of the difference in potential when switching from aqueous to organic electrolytes. It is reasonable to anticipate that the extent and effect of solvent ordering around redox centres in a monolayer will be generally different to that of the species in solution. Moreover, the possible coordination of OH^- ions by Os^{2+} in aqueous electrolyte might alter the electronic charge surrounding the metal centre in a way that leads to a decrease of the Os oxidation potential under these conditions.

The dielectric constant of the solvent can determine the extent of solvent ordering and the degree of insulation around the redox sites bound to the surface within the monolayer.[14a] In addition to that, different solvents can affect the thermodynamics of electron transfer to and from the molecule on the surface through differing degrees of insulating each molecule and also through the ability of the solvent to influence ion pairing within the monolayer. The dielectric constant of water (80) is far higher than that of acetonitrile (~36).[18] As water has the higher dielectric constant it may offer more insulation to the redox centres compared to acetonitrile thus reducing the degree of repulsive lateral interaction between adsorbates.

3.2.5.2 Surface Enhanced Raman Scattering Spectroscopy of Os(thimphen) Assembled on Au Electrodes

The vibrational modes of each mononuclear complex were also investigated using surface enhanced Raman scattering spectroscopy (SERS). A major advantage of SERS is the extent of enhancement of the Raman signal that is produced from the surface of the substrate. SERS focuses on the vibrational properties of molecules on a surface or very close to it as opposed to those of the bulk solution which allows for the investigation of any structural changes in molecules and their orientation when bound to surfaces. The SERS spectra of aqueous solutions of the ruthenium and osmium monomers were obtained using Au colloid as the source of enhancement for the Raman signal. The monolayers of each osmium complex were also analysed via SERS using roughened Au beads and Au slides as the substrate, the results of which are discussed below, Figure 3.29.

The Au colloid solution, originally pink in colour was mixed with an aqueous solution of each of the four monomers leading to a blue solution indicating that the metal complex has aggregated with the Au nano-particles in the Au colloid. The presence of the Au nano-particles leads to an enhancement of the Raman signal due to the two main contributions which include charge transfer and electromagnetic enhancement.[38] This is evident by comparing the spectrum of the Au colloid/metal complex mix with that of the metal complex in water alone where no Raman signal was obtained.

The SERS spectra of Os(thimphen) are shown in Figure 3.29 as well as that of $[Ru(bipy)_3]^{2+}$ which is included for comparison of the bipy stretching vibrations. Monolayers of this complex were formed on a Au bead and Au slide. The roughening of each of these substrates was required prior to deposition in order to achieve surface enhancement. Using a procedure [39] originally described by Tian *et al.* [40] the gold beads and slides were roughened in preparation for overnight deposition in solution of both of the osmium complexes. 0.1 M KCl solution was used as the electrolyte and each of the gold electrodes, following polishing and electrochemical cleaning in 0.5 M H_2SO_4, was prepared by scanning between potentials of -0.3 and 1.2 V, *vs.* SCE. The gold electrode was held at -0.3 V for 1.2 seconds and the potential then jumped to 1.2 V and was held there for 30 seconds. This was repeated 12 times using the multi-potential step function after which point the surface of the gold electrode appears rusty

brown in colour. The SERS spectra were recorded on a Perkin Elmer Raman station using a 785 nm laser.

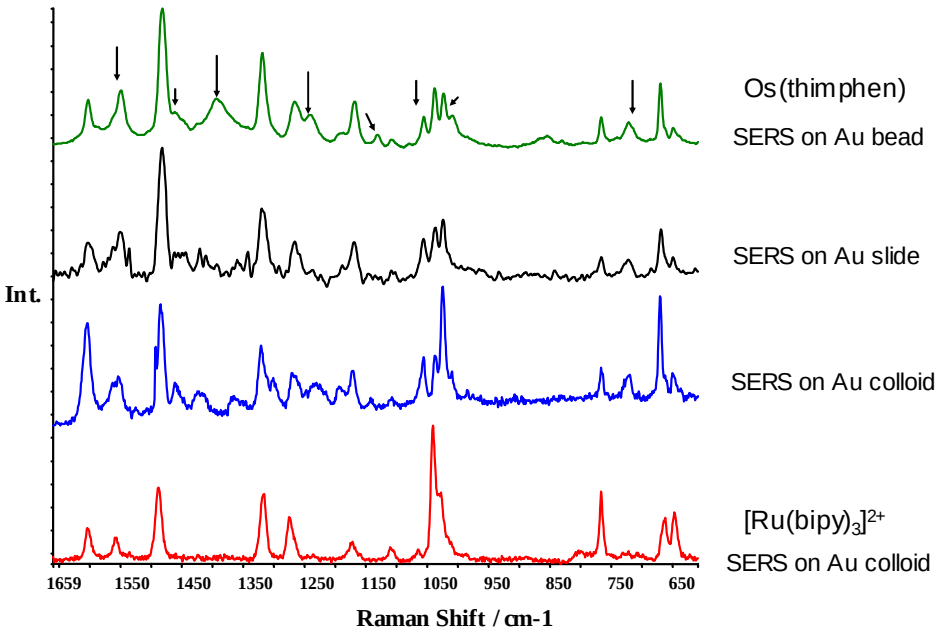

Figure 3.29: *SERS spectra of Os(thimphen) on a Au bead, Au slide and in Au colloid. The SERS spectrum of* $[Ru(bipy)_3]^{2+}$ *is included for comparison. The arrows indicate non-bipy bands.*

Comparing each of the four SERS spectra in Figure 3.29 a definite pattern emerges. The presence of signals related to the bipyridyl rings is recognised in each spectrum of the Os(thimphen) complex. These are compared with those signals of $[Ru(bipy)_3]^{2+}$ the spectrum of which is highlighted in red in the graph. The frequencies of each of the vibrational modes of the bipy ligands have been reported at 1608, 1563, 1491, 1320, 1276, 1264, 1176, 1043, 1028, 767 and 668 cm^{-1}.[32] The C-C stretching modes of the bipy ligand give rise to frequencies at 1608, 1563 and 1491 cm^{-1} with the ring modes occurring at 1028, 767 and 668 cm^{-1}. The C-H bend coupled with the ring stretch mode is represented by the band at 1176 cm^{-1}.[32, 36] Those peaks that are not related to the bipy vibrational modes, indicated by the arrows, must therefore be associated with vibrations from a different source. From electrochemical analysis it is

assumed that the Os(thimphen) complex is the only chemical species bound to the gold surface within the monolayer. Also, as the Raman cross section for water is low [39] it is assumed that the peaks in the spectrum obtained using Au colloid are solely related to the metal complex. It is therefore assumed that the signals in the spectrum that are not related to bipy appear as a result of vibrations associated with the thimphen ligand.

The Au bead and slide were soaked in a solution of the complex in ethanol. The SERS spectra obtained correspond to a monolayer of the complex on the substrate and this can be compared with the Au colloid where the complex is very close to the surface of the Au colloid but not bound. The SERS spectrum on the Au colloid portrays some differences to that of the spectra obtained for the monolayer of the complex. The orientation of the complex in the colloid is random whereas the orientation of the complex in the monolayer is more rigid. Two noted differences between the monolayer spectrum and that of the solution of the complex are the intensities of the peaks with frequencies at approximately 1600 and 1025 cm^{-1}. These bands are assigned as symmetric stretching modes from the bipy ligands and a possible reason for the difference in intensity may be due to the different orientation of the complex close to the Au nanoparticle as opposed to the monolayer of the complex. It is suggested that the complex forms the monolayer through the thiophene lone pair and as such the bipy ligands may be further away from the surface whereas with the Au nanoparticles the complex orientation for this spectrum may result from the bipy ligands located closer to the surface at that time.

Further experiments are required to conclusively assign all the signals arising from the vibrational modes of the thimphen ligand. SERS on the deuterated form of this complex would provide supporting information to that obtained here and lead to a more comprehensive and reliable study of the thimphen vibrational modes and their related frequencies. Although every signal in the spectrum cannot be assigned exactly with these results alone it can be stated that a monolayer of the complex does form on the Au substrate which is also confirmed in the electrochemistry of the monolayer on Au.

3.3 Conclusions

A series of ruthenium and osmium polypyridyl complexes, potentially useful as molecular transistors for molecular devices have been investigated, and their diffusion controlled and surface confined electrochemical properties have been examined. Each complex exhibits a single reversible metal centred oxidations and several reversible and irreversible ligand based reductions, Table 3.2. The first, least negative reduction of the M(pyrphen) complexes is quasi-reversible process that is dependent on the scan rate applied. Comparing the potential of this process with that of the first reduction of $[Ru(bipy)_3]^{2+}$, and factoring in its quasi-reversible nature, it is suggested that this process is centred on the pyrphen ligand itself whereas the first cathodic process of the M(thimphen) is thought to be localised on a bipyridyl ligand.

Reductive spectroelectrochemistry was carried out on both osmium complexes to further investigate this hypothesis. Bulk electrolysis at a potential sufficient to singly reduce the Os(thimphen) complex results in an observed decrease in the intensity of the bipy absorbance bands with the concomitant appearance of new absorbance bands in the region of the bipy anion radical (circa 330 nm, Figure 3.17). This result along with the electrochemical data suggests that the LUMO of the M(thimphen) complexes is located on a bipyridyl ligand. In contrast, the intensity of the absorbance bands associated with the bipy anion radical is far less for the reduced Os(pyrphen) complex, Figure 3.19. As the potential is gradually increased in the negative direction the intensities of these bands increases slightly. Although this evidence is not entirely conclusive, comparison of the absorbance spectra of the reduced complexes along with the electrochemical data implies that the LUMO level of the M(pyrphen) complexes is on the pyrphen ligand itself and not on a bipyridyl unit.

Excited state Raman spectroscopy of both ruthenium mononuclear complexes allows for the identification of the lowest lying excited state. Using a 9 ns pulse at 355 nm each complex was promoted to an electronically excited state, thus allowing the associated vibrational modes to be examined. This wavelength resonates with the associated absorbance wavelength of the bipy anion radical. It was found that vibrational modes of the bipy anion radical were observed in the excited state Raman spectra of both the Ru(thimphen) and Ru(pyrphen) which, surprisingly, suggests that

the lowest lying excited state involves a ^{3}MLCT transition localised on a bipyridyl ligand and not on the pyrphen or thimphen ligands. This is in contrast to the electrochemical and reductive spectroelectrochemical results which suggest that the LUMO of the M(pyrphen) complexes is not associated with a bipyridyl ligand.

Each of the four complexes has been spontaneously assembled on Pt and Au substrates. A linear relationship between the scan rate and the peak current suggest that the Faradaic response is associated with a complex on a surface and not that of a diffusion controlled process. The ΔE_p, FWHM and projected area per molecule, calculated from the surface coverage obtained, suggest that the monolayers of these complexes do not produce ideal electrochemical responses. The surface coverage calculated is within the range of that of a monolayer ($< 1.1 \times 10^{-10}$ mol cm^{-2}) however the FWHM of > 90.6 mV suggests that repulsive interactions exist between adsorbates on the surface. This is also supported by the projected area per molecule of each complex being greater than the area of the complex self.

The SERS spectra obtained for the Os(thimphen) complex (Figure 3.29), bound to a Au substrate and in a Au colloid solution also suggests that a monolayer is formed on the Au surface. There are noted differences between the SERS spectrum of the complex on a Au bead and that of the complex in Au colloid solution. The random orientation of the complex in the Au colloid leads to certain changes in certain bands associated with the bipy ligands. This may be as a result of the less rigid orientation in the colloid compared to the Au surface. It is proposed that the complex binds to the surface through the thiophene ring of the thimphen ligand. However to fully assign the non-bipy based vibrational modes as being solely associated with the thimphen ligand requires further experiments including SERS on the deuterated forms of the complex.

The properties of each mononuclear complex on a surface have been tentatively examined in this chapter. For these complexes to be classed as viable for use as molecular transistors their electron transfer rates and mechanisms of tunnelling current need to be examined. Further electrochemical analysis and *in situ* scanning tunnelling microscopy experiments would prove useful in reaching this goal.[13, 14]

3.4 Bibliography

1 Wiberg, E., Wiberg, N, Holleman, A.F., *Inorganic Chemistry*, Academic Press, New York, USA, **2001**.

2 Seddon, E.A., Seddon, K.R., *The Chemistry of Ruthenium*, Elsevier, Amsterdam, The Netherlands, **1984**.

3 Cotton, F.A., Wilkinson, G., Gaus, P.L., *Basic Inorganic Chemistry*, 3rd Ed., John Wiley & Sons, New York, USA, **1995**.

4 (a) Balzani, V., Juris, A., Venturi, M., Campagna, S., Serroni, S., *Chem. Rev.*, **1996**, *96*, 759, (b) Juris, A., Balzani, V., Barigelletti, F., Campagna, S., Belser, P., Von Zelewsky, A., *Coord. Chem. Rev.*, **1988**, *84*, 85, (c) Balzani, V., Campagna, S., Denti, G., Juris, A., Ventura, M., *Coord. Chem. Rev.*, **1994**, *132*, 1, (d) Balzani, V., Campagna, S., Denti, G., Juris, A., Serroni, S., Venturi, M, *Acc. Chem. Res.*, **1998**, *31*, 26, (e) Sauvage, J.P., Collin, J.P., Chambron, J.C., Guillerez, S., Coudret, C., *Chem. Rev.*, **1994**, *94*, 993.

5 Paris, J.P., Brandt, W.W., *J. Am. Chem. Soc.*, **1959**, *81*, 5001.

6 (a) Balzani, V., Credi, A., Venturi, M., *Molecular Devices and Machines - A Journey into the Nano World*, Wiley-VCH, Weinheim, Germany, **2003**, (b) Lundstrom, M, *Science*, **2003**, *299*, 210, (C) Packan, P. A., *Science*, **1999**, *285*, 2079.

7 Low, P.J., *Dalton Trans*, **2005**, 2821.

8 Tour, J.M., *Acc. Chem. Res.*, **2000**, *33*, 791.

9 Feynman, R.P., *Eng. Sci.*, **1960**, *23*, 22.

10 (a) Bumm, L.A., Arnold, J.J., Cygan, M.T., Dunbar, T.D., Burgin, T.P., Jones, L., Allara, D.L., Tour, J.M., Weiss, P.S., *Science*, **1996**, *271*, 1705, (b) Tans,

S.J., Devoret, M.H., Dai, H.J., Thess, A., Smalley, R.E., Geerligs, L.J., Dekker, C., *Nature*, **1997**, *386*, 474.

11 (a) Zhitenev, N.B., Meng, H., Bao, Z., *Phys. Rev. Lett.*, **2002**, *88*, 226801-1, (b) Park, J., Pasupathy, A.N., Goldsmith, J.I., Chang, C., Yaish, Y., Petta, J.R., Rinkoshi, M., Sethna, J.P., Abruna, H.D., McEuen, P.L., Ralph, D.C., *Nature*, **2002**, *417*, 722, (c) Kubatkin, S., Danilov, A., Hjort, M., Cornil, J., Bredas, J.L., Stuhr-Hansen, N., Hedegard, P., Bjornholm, T., *Nature*, **2003**, *425*, 698.

12 (a) Reed, M.A., *Proc. IEEE*, **1999**, *87*, 652, (b) Metzger, R.M., *Chem. Rev.*, **2003**, *103*, 3803, (c) Ng, M.K., Lee, D.C., Yu, L., *J. Am. Chem. Soc.*, **2002**, *124*, 11862.

13 (a) Albrecht, T., Guckian, A., Ulstrup, J., Vos, J.G., *IEEE Transactions on Nanotechnology*, **2005**, *4*, 430, (b) Albrecht, T., Guckian, A., Ulstrup, J., Vos, J.G., *Nano Letters*, **2005**, *5*, 1451, (c) Albrecht, T., Moth-Poulsen, K., Christensen, J.B., Guckian, A., Bjornholm, T., Vos, J.G., Ulstrup, J., *Faraday Discussions*, **2006**, *131*, 265, (d) Albrecht, T., Guckian, A., Kuznetsov, A.M., Vos, J.G., Ulstrup, J., *J. Am. Chem. Soc.*, **2006**, *128*, 17132.

14 (a) Forster, R.J., Faulkner, L.R., *J. Am. Chem. Soc.*, **1994**, *116*, 5444, (b) Forster, R.J., Faulkner, L.R., *J. Am. Chem. Soc.*, **1994**, *116*, 5453.

15 (a) Forster, R.J., Figgemeier, E., Lees, A., Hjelm, J., Vos, J.G., *Langmuir*, **2000**, *16*, 7867, (b) Forster, R.J., O'Kelly, J.P., *J. Electrochem. Soc.*, **2001**, *148*, 31.

16 Forster, R.J., Faulkner, L.R., *Anal. Chem.*, **1995**, *67*, 1232.

17 Bard, A.J., Faulkner, L.R., *Electrochemical Methods, Fundamentals and Applications 2nd Edition*, John Wiley & Sons, Inc., New Jersey, USA, **2001**.

18 Sawyer, D.T., Sobkowiak, A., Roberts Jr., J. L., *Electrochemistry for chemists 2nd Edition*, John Wiley & Sons Ltd., New York, USA, **1995**.

19 Hibbert, D.B., *Introduction to Electrochemistry*, MacMillan Press Ltd., London, UK, **1993**.

20 Hage, R., Ph.D. Thesis, Leidin University, The Netherlands, **1991**.

21 Wu, J.Z., Ye, B.H., Wang, L., Ji, L.N., Zhou, J.Y., Li, R.H., Zhou, Z.Y., *J. Chem. Soc., Dalton Trans.*, **1997**, 1395.

22 Cooke, M.M., Doeven, E.H., Hogan, C.F., Adcock, J.L., McDermott, G.P., Conlon, X.A., Barnett, N.W., Pfeffer, F.M., Francis, P.S., *Analytica Chimica Acta*, **2009**, *635*, 94.

23 Roffia, S., Casadei, R., Paolucci, F., Paradisi, C., Bignozzi, C.A., Scandola, F., *J. Electroanal. Chem.*, **1991**, *302*, 157.

24 Skoog, D.A., Holler, F.J., Nieman, T.A., *Principles of Instrumental Analysis*, Harcourt Brace & Company, Florida, USA, **1998**.

25 Lide, D.R., *Handbook of Organic Solvents*, CRC Press, Florida, USA, **1995**.

26 Flick, E.W., *Industrial Solvents Handbook 5th Ed.*, New Jersey, USA, **1998**.

27 Dini, D., Decker, F., Zotti, G., Schiavon, G., Zecchin, S., Andreani, F., Salatelli, E, *Chem. Mater.*, **1999**, *11*, 3484.

28 Heath, G.A., Yellowlees, L.J., *J.C.S. Chem. Comm.*, **1981**, 287.

29 Keyes, T.E., Forster, R.J., *Handbook of Electrochemistry*, Ed. C.G. Zoski, Elsevier Science, **2007**.

30 Browne, W.R., O'Boyle, N.M., McGarvey, J.J., Vos, J.G., *Chem. Soc. Rev.*, **2005**, *34*, 641.

31 Treffert-Ziemelis, S.M., Golus, J., Strommebt, D.P., Kincaid, J.R., *Inorg. Chem.*, **1993**, *32*, 3890.

32 Mallick, P.K., Danzer, G.D., Strommen, D.P., Kincaid, J.R., *J. Phys. Chem.*, **1988**, *92*, 5628.

33 Forster, R.J., Keyes, T.E., Vos, J.G., *Interfacial Supramolecular Assemblies*, John Wiley & Sons Ltd., Chichester, England, **2003**.

34 Finklea, H.O., *Self Assembled Monolayers on Electrodes, Encyclopaedia of Analytical Chemistry*, Vol. 11, Wiley, Chicester, UK, **2000**.

35 Bertoncello, P., Kefalas, E.T., Pikramenou, Z., Unwin, P.R., Forster, R.J., *J. Phys. Chem. B*, **2006**, *110*, 10063.

36 Forster, R.J., Pellegrin, Y., Leane, D., Brennan, J.L., Keyes, T.E., *J. Phys. Chem. C*, **2007**, *111*, 2063.

37 Goodwin, H.A., Kepert, D.L., Patrick, J.M., Skelton, B.W., White, A.H., *Aust. J. Chem.*, **1984**, *37*, 1817.

38 Ren, B., Yao, J.L., Li, X.Q., Cai, W.B., Mao, B.W., Tian, Z.Q., *Internet J. Vib. Spec.*, **2004**, *1*, 21.

39 Abdelsalam, M.E., Bartlett, P.N., Baumberg, J.J., Cintra, S., Kelf, T.A., Russell, A.E., *Electrochem. Comm.*, **2005**, *7*, 740.

40 Tian, Z.Q., Ren, B., Wu, D.Y., *J. Phys. Chem. B*, **2002**, *106*, 9463.